Molecular Catalysis 504 (2021) 111451

Contents lists available at ScienceDirect

Molecular Catalysis

journal homepage: www.journals.elsevier.com/molecular-catalysis

Chemoenzymatic enantioselective and stereo-convergent syntheses of lisofylline enantiomers *via* lipase-catalyzed kinetic resolution and optical inversion approach

Paweł Borowiecki [a,*], Beata Zdun [a], Maciej Dranka [b]

[a] Warsaw University of Technology, Department of Drugs Technology and Biotechnology, Laboratory of Biocatalysis and Biotransformations, Koszykowa St. 75, 00-662, Warsaw, Poland
[b] Warsaw University of Technology, Faculty of Chemistry, Department of Inorganic Chemistry and Solid State Technology, Noakowskiego 3, 00-664, Warsaw, Poland

ARTICLE INFO

Keywords:
Enantiomeric lisofylline
Biocatalysis
Lipases
Kinetic resolution
Stereo-convergent syntheses
Stereoinversion
XRD analyses
Docking studies

ABSTRACT

Highly enantioselective enzymatic kinetic resolution (EKR) of racemic lisofylline is presented for the first time. A comprehensive optimization of the key parameters of lipase-catalyzed transesterification of racemic lisofylline revealed that optimal biocatalytic system consisted of immobilized lipase type B from *Candida antarctica* (Chirazyme L-2, C-3) suspended in a mixture of 3 equiv of vinyl acetate as an acetyl donor and ethyl acetate as a solvent. Under optimal reaction conditions, the 1 g-scale (Chirazyme L-2, C-3)-catalyzed kinetic resolution of racemic lisofylline furnished both the EKR products in a homochiral form (>99 % ee) with the 50 % conv., and the highest possible enantioselectivity. The best results in terms of the reaction yields (47–50 %) and enantiomeric purity of the kinetically-resolved optically active products were achieved when the preparative-scale EKR was carried out for 2 h at 60 °C. In addition, stereoinversion of the less biologically-relevant (*S*)-lisofylline into its (*R*)-enantiomer was successfully achieved *via* acetolysis of the respective optically pure (*S*)-mesylate by using 2 equiv of ceasium acetate and catalytic amount of 18-Crown-6 in dry toluene, followed by K_2CO_3-mediated methanolysis of (*R*)-acetate. The elaborated EKR methodology together with enantioconvergent strategy provided a useful chemoenzymatic protocol for the synthesis of complementary enantiomers of titled API. Moreover, we report on the first single-crystal X-ray diffraction (XRD) analyses performed for the synthesized lisofylline enantiomers. Insight into the source of CAL-B stereoselectivity toward racemic lisofylline was gained by molecular docking experiments. *In silico* theoretical predictions matched very well with experimental results.

1. Introduction

The most common methylxanthines are secondary plant metabolites derived from purine nucleotides, among which caffeine **I**, theobromine **II**, theophylline **III**, 7-methylxanthine **IV**, and paraxanthine **V** can be found in plant tissues in the highest concentrations (Fig. 1A). Due to the versatility of biological and pharmaceutical activities [i.e. inhibitory activity against tissue phosphodiesterases (PDEs), antagonistic properties toward adenosine receptors (A_1, A_{2A}, A_{2B} and A_3), potential of reducing intracellular calcium ions release, activation of histone deacetylases (HDACs)] [1] methylxanthines are consensually identified nowadays as one of the major important structural motifs used in drug development. Methylxanthines are especially appreciated for being very efficient broncho- and vaso-dilators as well as anti-inflammatory and immunomodulatory agents, respectively. Several pharmaceutically relevant compounds possessing xanthine moiety, mostly approved for the treatment of chronic pulmonary disorders and/or coronary, cerebrovascular and peripheral arterial diseases, are as follows: proxyphylline **VI**, enprophylline **VII**, aminophylline **VIII**, diprophylline **IX**, xanthinol **X**, reproterol **XI**, acebrophylline **XII**, doxofylline **XIII**, pentifylline **XIV**, bamifylline **XV**, furafylline **XVI**, arofylline **XVII**, dasantafil **XVIII**, and dimenhydrinate **XIX** (Fig. 1B). The other xanthine-like pharmaceutically active molecules with various clinical indications and only few side effects include: propentofylline **XX**, pentoxifylline **XXI**, and lisofylline **XXII** (Fig. 1C).

The prominent example among the above-mentioned derivatives of the methylxanthine theobromine is lisofylline [LSF, namely 1-(5*R*-hydroxyhexyl)-3,7-dimethyl-3,7-dihydro-1*H*-purine-2,6-dione or 1-(5*R*-

* Corresponding author.
E-mail addresses: pawel_borowiecki@onet.eu, pborowiecki@ch.pw.edu.pl (P. Borowiecki).

https://doi.org/10.1016/j.mcat.2021.111451
Received 9 October 2020; Received in revised form 9 January 2021; Accepted 30 January 2021
Available online 21 February 2021

hydroxyhexyl)-3,7-dimethylxanthine], which constitutes a unique pharmacologically active metabolite of pentoxifylline [2,3]. Lisofylline was originally developed by Cell Therapeutics, Inc. (Seattle, WA) to prevent the onset of experimental autoimmune encephalomyelitis (EAE) [4] as well as to eliminate incidence of graft-versus-host disease (GVHD) [5]. LSF is a powerful molecule exhibiting strong anti-inflammatory and immunomodulatory properties by inhibiting PDE (mainly PDE4B and PDE7 isoenzymes) [6,7] as well as blocking interleukin-12 (IL-12) signaling pathways [i.e. IL-12-induced T helper 1 (Th1) differentiation] and the activation of the signal transducer and activator of transcription 4 (STAT-4) gene associated with the production of immune-dependent proteins [8].

Moreover, anti-inflammatory action of lisofylline additionally stems from suppressing the production of several other pro-inflammatory cytokines, including interleukin-1 (IL-1), interferon-gamma (IFN-γ) or tumor necrosis factor-alpha (TNF-α). Therefore, it has been investigated as a promising drug candidate for acute respiratory distress syndrome (RDS), oxidative acute lung injury, mucositis, septic shock, severe sepsis, hemorrhagic organ injury (i.e. hepatic injury), ischemic reperfusion, and hypoxia [9–12]. Recent studies on biological activities of lisofylline have revealed that it promotes hematopoiesis after chronic blood cell depression following high-dose chemotherapy of tumors, and thus it might be useful in attenuating the side effects (i.e. neutropenic infections) of cytotoxic cancer treatment in general [13,14]. Lisofylline has been shown to inhibit activity of myeloperoxidase (MPO) and interleukin-18 (IL-18) proteins, both involved in inflammatory bowel disease (i.e. Crohn's disease) responsible for the colitis fibrogenesis [15]. Lisofylline has also shown beneficial effects in protecting pancreatic *β*-cells and islets of the Langerhans from multiple (pro-inflammatory cytokine)-mediated damages due to its ability to restore both the insulin secretion capability and INS-1 cell viability [16]. The above-mentioned features of lisofylline may result from promotion of mitochondrial metabolism of INS-1 cells as well as efficient inhibition of nuclear DNA breakage under influence of inflammatory cytokines, and in this context it is envisioned to constitute high therapeutic potency in effective prevention and treatment of insulin-dependent Type 1 *diabetes mellitus* and/or after islet cell transplantation [17,18].

The pharmacokinetic and pharmacodynamic studies conducted with both the enantiomers of lisofylline have revealed that only the (*R*)-enantiomer is responsible for desired pharmacological activity, whereas its antipode remains inactive. Moreover, (*R*)-configurated lisofylline is several hundred-fold more potent at inhibiting the activity of inflammatory cytokines than its parent molecule, pentoxifylline [19]. Finally, biotransformation of pentoxifylline to lisofylline *in vitro* and *in vivo* in humans is unfortunately highly stereoselective in favor of the (*S*)-enantiomer formation [20]. Undesired metabolism of pentoxifylline can be converted by administration of this drug together with ciprofloxacin [21]. Nevertheless, such a therapeutic tactic seems to be highly disadvantageous.

Given its useful pharmaceutical properties, (*R*)-lisofylline has attracted a great deal of attention from synthetic laboratories. Therefore, in the last two decades several chemical methods have been developed for the synthesis of enantiomerically enriched (*R*)-lisofylline using commercially available chiral building blocks {i.e. (*S*)-lactic acid ethyl

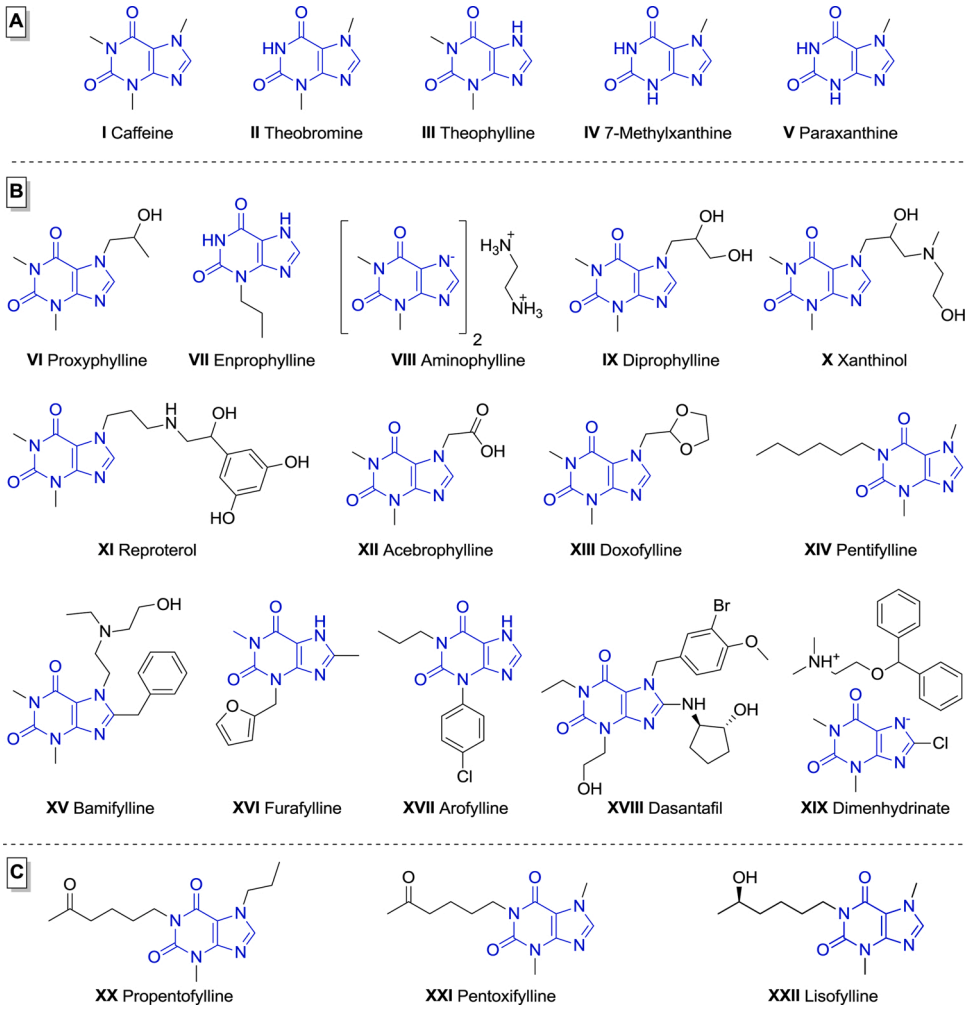

Fig. 1. Examples of natural products (**I**–**V**) and pharmaceuticals (**VI**–**XXII**) containing xanthine moiety.

ester [22] or 5-(*R*)-acetoxy-1-chlorohexane [23]} or chiral auxiliaries {i.e. (–)-pinane diol obtained from natural (–)-β-pinene [24]}. One of the few strategies used to synthesize this molecule in enantioselective fashion involves an asymmetric catalytic hydrogenation of racemic ethyl 5-hydroxyhexanoate into (*R*)-hexane-1,5-diol (91 % ee) using chiral iridium-complexes [Ir-(*R*)-SpiroPAP] under kinetically-controlled conditions [25,26]. Disappointingly, the authors of this publication did not provide any data concerning optical purity of the desired enantiomeric drug. The other synthetic method reported on the employment of the Jacobsen hydrolytic kinetic resolution (J-HKT) of racemic 2-(4-bromobutyl)oxirane in the presence of (*R,R*)-(−)-*N,N′*-bis(3,5-di-*tert*-butylsalicylidene)-1,2-cyclohexanediaminocobalt(II) [27]. In this case, J-HKT-based strategy allowed to obtain (*S*)-6-bromohexane-1,2-diol, which after one-pot boron-catalyzed regioselective mono-deoxygenation/silylation procedure using $B(C_6F_5)_3/Et_3SiH/Ph_2SiH_2$-system, followed by the alkylation of theobromine, yielded enantiomerically pure (*R*)-lisofylline (>99 % ee).

In addition to chemical methods, alternative biocatalytic approaches have also been developed. In fact, bioreduction of pentoxifylline to LSF was firstly reported with *Rhodotorula rubra* (ATCC 20,129) [28], although this process proceeded under low reaction rates (92 % conv. after 144 h) in moderate 40 % yield and with an unknown stereochemistry outcome. More recent studies with *Rhodotorula rubra* DSM 5436 [29,30] have shown the production of (*S*)-lisofylline (>98 % ee), which then had to be converted into its antipode using Mitsunobu reaction. Among highly (*R*)-stereoselective bioreductions particularly noteworthy are microbial whole-cell systems consisting of *Lactobacillus kefiri* DSM 20,587 [31,32] and *Saccharomyces cerevisiae* (wine yeast) [33], respectively. Both these methods yielded (*R*)-lisofylline in 98 % ee and very high 95–100 % conv. within 24 h or 72 h, respectively. Nevertheless, it is somewhat surprising that the isolated yields of the biotransformation products were omitted. On the other hand, some promising biocatalytic methods were reported that employ isolated enzymes such as (*R*)-specific alcohol dehydrogenase from *Lactobacillus kefiri* (*LKADH*) [34] leading to (*R*)-lisofylline in 98 % ee and total >99 % conv. (again with only 'HPLC yield' given). Last but not least, mutated human cytochrome P450 3A4 monooxygenases [35,36] was verified as a potential biocatalysts for chemo- and stereo-selective hydroxylation of 1-hexyl-3,7-dimethyl-3,7-dihydro-1*H*-purine-2,6-dione (namely, 1-*N*-hexyl-theobromine). However, this strategy suffers from low 40 % ee of (*R*)-lisofylline isolated in 63 % yield.

Although considerable attention has been devoted to the development of efficient methods for the enantioselective synthesis of optically active (*R*)-lisofylline in recent decades, this task still remains an open challenge for organic chemists as the traditional synthetic routes are rather complex and time-consuming, while chemocatalytic procedures relying on metalocatalysts, even if consisting of less reaction steps, still suffer from serious limitations, such as harsh reaction conditions (i.e. high pressures of H_2 gas) and significant implications for the environment due to their high toxicity. In turn, despite the many advantages that biocatalytic methods offer in the synthesis of (*R*)-lisofylline, certain drawbacks including low substrate loading and relatively low volumetric productivity as well as complicated downstream processing, make their industrial application is significantly constrained. In order to circumvent the above-mentioned limitations as well as to augment biocatalytic toolbox for the synthesis of enantiomeric (*R*)-lisofylline, here we elaborate on a simple and straightforward preparative-scale chemoenzymatic synthesis of both enantiomers of titled API using lipases as biocatalysts for kinetic resolution of the respective racemate coupled with optical inversion of the waste (*S*)-stereoisomer.

2. Experimental

2.1. General experimental methods

Reagents and solvents were purchased from various commercial sources (Sigma Aldrich, Alfa Aesar, POCH) and were used without further purification. High-performance liquid chromatography HPLC-grade solvents (*n*-hexane and 2-PrOH) were purchased from POCH (Poland). Evaporation of the solvent residues was performed at reduced pressure by means of Büchi rotary evaporator and high-vacuum oil pump at $p = 0.05$ mmHg. Melting points, uncorrected, were determined with a commercial apparatus (Thomas-Hoover "UNI-MELT" capillary melting point apparatus) on samples contained in rotating glass capillary tubes open on one side (1.35 mm inner diam. and 80 mm length). Analytical thin-layer chromatography was carried on TLC aluminum plates (Merck) covered with silica gel of 0.2 mm thickness film containing a fluorescence indicator green 254 nm (F_{254}) and using UV light as a visualizing agent. Preparative separations were carried out by: (i) column chromatography using thick-walled glass columns and silica gel (230–400 mesh) with grain size 40–63 μm purchased from Merck, Germany. The chromatographic analyses (GC) were performed with a Agilent Technologies 6890 N instrument equipped with a flame ionization detector (FID) and fitted with HP-50+ (30 m) semipolar column (50 % phenyl – 50 % methylpolysiloxane); Helium (2 mL/min) was used as carrier gas; retention times (t_R) are given in minutes under these conditions. The enantiomeric excesses (% ee) of kinetic resolution products were determined by HPLC analysis performed on Shimadzu CTO-10ASV chromatograph equipped with STD-20A UV detector and Chiralcel OD—H chiral column (4.6 mm × 250 mm, 5 μm grain size from Daicel Chemical Ind., Ltd.) or Chiralpak AD—H (4.6 mm × 250 mm, 5 μm grain size from Daicel Chemical Ind., Ltd.) both equipped with a pre-column (4 mm × 10 mm, 5 μm) using mixtures of *n*-hexane/2-PrOH as mobile phase in the appropriate ratios given in experimental section [both the mobile phase composition as well as the flow rate were fine tuned for each analysis (see Supporting Information, Table S4)]; the wavelength of UV detection was set at 273 nm; the HPLC analyses were executed in an isocratic and isothermal (30 °C) manner. Optical rotations ([α]) were measured with a PolAAr 32 polarimeter in a 2 dm long cuvette using the sodium D line ($\lambda = 589$ nm); the units of the specific rotation are: (deg × mL)/(g × dm). ^{1}H NMR (500 MHz) and ^{13}C NMR (126 MHz) spectra were recorded on a Varian NMR System 500 MHz spectrometer; ^{1}H and ^{13}C chemical shifts (δ) are reported in parts per million (ppm) relative to the solvent signals [$CDCl_3$, δ_H (residual $CHCl_3$) 7.26 ppm, δ_C 77.16 ppm]. Chemical shifts are quoted as s (singlet), d (doublet), dd (doublet of doublets), t (triplet), q (quartet), m (multiplet), and br s (broad singlet); coupling constants (*J*) are reported in Hertz. Mass spectrometry was recorded on Micro-mass ESI Q-TOF spectrometer with MSI concept 1H (EI, 70 eV ionization) for MS analysis and on Q Exactive Hybrid Quadrupole-Orbitrap Mass Spectrometer, ESI source: electrospray with spray voltage 4.00 kV for FTMS analysis; all samples were prepared by dilution of MeOH (0.5 mL) and additives of mixtures of $CH_3CN/MeOH/H_2O$ (50:25:25, v/v/v) + 0.5 % formic acid (HCO_2H) each.

2.2. General procedure for the synthesis of racemic lisofylline (rac-2)

To a solution of pentoxifylline (**1**, 2 g, 7.19 mmol) in MeOH (40 mL) and CH_2Cl_2 (6 mL) cooled to 0–5 °C, $NaBH_4$ (816 mg, 21.56 mmol) was added portionwise over 40 min. The reaction mixture was stirred in the cold for 2.5 h, and afterwards, it was stopped by evaporation the solvent to dryness under reduced pressure. The residual slurry was diluted with H_2O (200 mL) and extracted with EtOAc (3 × 150 mL). The combined extracts were rinsed with brine (100 mL), dried with anhydrous $MgSO_4$, the drying agent was filtered off, and the permeate was condensed under reduced pressure to give product *rac*-**2** (1.69 g, 6.03 mmol, 84 %) as a white solid. Mp 123–125 °C (EtOAc) [lit. [25] 123–125 °C (EtOAc)]; R_f [$CHCl_3$/MeOH (95:5, v/v)] 0.27; ^{1}H NMR (500 MHz, $CDCl_3$): δ 1.16 (d, $J = 6.1$ Hz, 3 H), 1.31–1.56 (m, 4 H), 1.58–1.71 (m, 2 H), 1.82 (br. s., 1 H), 3.55 (s, 3 H), 3.74–3.83 (m, 1 H), 3.96 (s, 3 H), 3.99 (t, $J = 7.5$ Hz, 2 H), 7.49 (s, 1 H); ^{13}C NMR (126 MHz, $CDCl_3$): δ 23.0, 23.6, 28.0, 29.8, 33.7, 38.9, 41.3, 67.9, 107.8, 141.5, 148.9, 151.6, 155.5; IR (nujol): ν_{max} =

3364, 3112, 1697, 1656, 1601, 1548, 1449, 1410, 1318, 1283, 1232, 1185, 1159, 1132, 1080, 1060, 1000, 978, 936, 882, 841, 812, 764, 752; MS (ESI-TOF) *m/z*: $[M+H]^+$ Calcd for $C_{13}H_{21}N_4O_3^+$ *m/z*: 281.1609, Found 281.1387, $[2M+H]^+$ $C_{26}H_{41}N_8O_6^+$ *m/z*: 561.3144, Found 561.3820; MS (ESI-TOF) *m/z*: $[M-H]^-$ Calcd for $C_{13}H_{19}N_4O_3^-$ *m/z*: 279.1462, Not Found, $[M+2Na-H]^-$ Calcd for $C_{13}H_{19}N_4Na_2O_3^-$ *m/z*: 325.1258, Found 325.1687, $[2M+2Na-H]^-$ Calcd for $C_{26}H_{39}N_8Na_2O_6^-$ *m/z*: 605.2793, Found 605.3885; FTMS (ESI-TOF) *m/z*: $[M+H]^+$ Calcd for $C_{13}H_{21}N_4O_3^+$ *m/z*: 281.1609, Found 281.1605; GC [240–260 (10 °C/min)]: t_R =11.99 min or GC [260 (const.)]: t_R = 8.77 min; UV/VIS: λ_{max} = 273 nm (EtOH); HPLC [*n*-hexane-EtOH (90:10, v/v); f = 0.3 mL/min; λ = 273 nm; *T* = 25 °C (Chiralcel OD-H)]: t_R = 112.23 (*R*-isomer) and 119.04 min (*S*-isomer); HPLC [*n*-hexane-2-PrOH (78:22, v/v); f = 1.0 mL/min; λ = 273 nm; *T* = 25 °C (Chiralpak AD-H)]: t_R = 30.59 (*R*-isomer) and 33.37 min (*S*-isomer).

2.3. General procedure for the synthesis of racemic esters of lisofylline *rac-3a–d*

To a solution of lisofylline (*rac*-**2**, 100 mg, 0.36 mmol) in CH_2Cl_2 (5 mL), Et_3N (54 mg, 0.54 mmol, 75 μL, 1.5 equiv) and DMAP (10 mg) were added. The mixture was cooled to 0–5 °C in ice bath. Next, one of the appropriate acyl chlorides (1.5 equiv) was dissolved in dry CH_2Cl_2 (2.5 mL) and added dropwise to the reaction mixture by using syringe. Afterwards, the resulting mixture was continuously stirred at cooling bath temperature and left to warm at room temperature for next 24 h. The crude mixture was diluted with CH_2Cl_2 (10 mL), subsequently quenched with H_2O (20 mL), the water phase was extracted with CH_2Cl_2 (3 × 10 mL), and the combined organic layer was washed with saturated aqueous solution of $NaHCO_3$ (40 mL), brine (40 mL), and dried over anhydrous $MgSO_4$. After filtration of the drying agent under suction and subsequent evaporation of the residuals of solvent under reduced pressure the crude product was purified by column chromatography on silica gel, using gradient of $CHCl_3$/MeOH (99:1, 98:2, 95:5 v/v) mixture, thus obtaining desired esters *rac*-**3a**–**d**.

2.3.1. 6-(3,7-Dimethyl-2,6-dioxo-2,3,6,7-tetrahydro-1H-purin-1-yl) hexan-2-yl acetate (lisofylline acetate, rac-3a)

Yield 40 % (46 mg); colorless oil (*rac*-**3a**); white solid [(*R*)-(+)-**3a**]: Mp 82–85 °C ($CHCl_3$/MeOH); R_f [$CHCl_3$/MeOH (95:5, v/v)] 0.51; ^{1}H NMR (500 MHz, $CDCl_3$): δ 1.20 (d, *J* = 5.9 Hz, 3 H), 1.30–1.47 (m, 2 H), 1.49–1.69 (m, 4 H), 2.01 (s, 3 H), 3.56 (s, 3 H), 3.92–4.06 (m, 5 H), 4.79–4.97 (m, 1 H), 7.49 (s, 1 H); ^{13}C NMR (126 MHz, $CDCl_3$): δ 20.0, 21.5, 22.9, 28.0, 29.8, 33.7, 35.7, 41.3, 71.0, 110.2, 141.5, 148.9, 151.6, 155.4, 170.9; IR (nujol): ν_{max} = 3507, 3112, 2948, 2867, 1729, 1706, 1657, 1604, 1552, 1487, 1456, 1417, 1372, 1321, 1248, 1191, 1130, 1086, 1019, 952, 764; MS (ESI-TOF) *m/z*: $[M+H]^+$ Calcd for $C_{15}H_{23}N_4O_4^+$ *m/z*: 323.1714, Found 323.1614; FTMS (ESI-TOF) *m/z*: $[M+H]^+$ Calcd for $C_{15}H_{23}N_4O_4^+$ *m/z*: 323.17138, Found 323.17089; GC [240–260 (10 °C/min)]: t_R = 11.99 min or GC [260 (const.)]: t_R = 8.77 min; UV/VIS: λ_{max} = 273 nm (EtOH); HPLC [*n*-hexane-2-PrOH (78:22, v/v); f = 1.0 mL/min; λ = 273 nm; *T* = 25 °C (Chiralpak AD-H)]: t_R = 13.98 (*S*-isomer) and 17.26 min (*R*-isomer).

2.3.2. 6-(3,7-Dimethyl-2,6-dioxo-2,3,6,7-tetrahydro-1H-purin-1-yl) hexan-2-yl butanoate (lisofylline butanoate, rac-3b)

Yield 43 % (54 mg); colorless oil; R_f [$CHCl_3$/MeOH (95:5, v/v)] 0.45; ^{1}H NMR (500 MHz, $CDCl_3$): δ 0.92 (t, *J* = 7.5 Hz, 3 H), 1.18 (d, *J* = 6.4 Hz, 3 H), 1.30–1.46 (m, 2 H), 1.49–1.71 (m, 6 H), 2.23 (t, *J* = 7.5 Hz, 2 H), 3.55 (s, 3 H), 3.93–4.02 (m, 5 H), 4.88 (dd, *J* = 12.7, 6.1 Hz, 1 H), 7.49 (s, 1 H); ^{13}C NMR (126 MHz, $CDCl_3$): δ 13.8, 18.7, 20.1, 23.0, 28.0, 29.8, 33.7, 35.8, 36.7, 41.3, 70.7, 107.8, 141.5, 148.9, 151.6, 155.4, 173.5; IR (nujol): ν_{max} = 3113, 2960, 2867, 1709, 1656, 1605, 1548, 1485, 1453, 1352, 1241, 1187, 1140, 1089, 1007, 982, 950, 881, 849, 802, 760, 653; FTMS (ESI-TOF) *m/z*: $[M+H]^+$ Calcd for $C_{17}H_{27}N_4O_4^+$ *m/z*: 351.20268, Found 351.20213; GC [260 (const.)]: t_R = 15.84 min; UV/VIS: λ_{max} = 274 nm (EtOH); HPLC [*n*-hexane-2-PrOH (78:22, v/v); f = 1.0 mL/min; λ = 273 nm; *T* = 25 °C (Chiralpak AD-H)]: t_R=10.12 (*S*-isomer) and 12.99 min (*R*-isomer).

2.3.3. 6-(3,7-Dimethyl-2,6-dioxo-2,3,6,7-tetrahydro-1H-purin-1-yl) hexan-2-yl decanoate (lisofylline decanoate, rac-3c)

Yield 36 % (56 mg); yellowish oil; R_f [$CHCl_3$/MeOH (95:5, v/v)] 0.47; ^{1}H NMR (500 MHz, $CDCl_3$): δ 0.82–0.92 (m, 3 H), 1.17–1.21 (m, 3 H), 1.23–1.31 (m, 12 H), 1.32–1.47 (m, 2 H), 1.51–1.70 (m, 6 H), 2.21–2.29 (m, 2 H), 3.57 (s, 3 H), 3.96–4.02 (m, 5 H), 4.89 (dd, *J* = 12.8, 6.2 Hz, 1 H), 7.50 (s, 1 H); ^{13}C NMR (126 MHz, $CDCl_3$): δ 14.2, 20.1, 22.8, 23.0, 25.2, 28.0, 29.3, 29.4, 29.6, 29.8, 32.0, 33.7, 34.9, 35.8, 41.3, 44.8, 70.7, 107.8, 141.5, 148.9, 151.6, 155.4, 173.7; IR (nujol): ν_{max} = 3513, 3116, 1706, 1664, 1604, 1548, 1490, 1414, 1360, 1328, 1280, 1239, 1181, 1127, 1111, 764, 752; FTMS (ESI-TOF) *m/z*: $[M+H]^+$ Calcd for $C_{23}H_{39}N_4O_4^+$ *m/z*: 435.29658, Found 435.29607; GC [260 (const.)]: Not Found; UV/VIS: λ_{max} = 273 nm (EtOH); HPLC [*n*-hexane-2-PrOH (78:22, v/v); f = 1.0 mL/min; λ = 273 nm; *T* = 25 °C (Chiralpak AD-H)]: t_R=7.75 (*S*-isomer) and 9.70 min (*R*-isomer).

2.3.4. 6-(3,7-Dimethyl-2,6-dioxo-2,3,6,7-tetrahydro-1H-purin-1-yl) hexan-2-yl hexadecanoate (lisofylline palmitate, rac-3d)

Yield 48 % (89 mg); yellowish oil (*rac*-**3d**); white solid [(*R*)-(+)-**3d**]: Mp 39–42 °C ($CHCl_3$/MeOH); R_f [$CHCl_3$/MeOH (95:5, v/v)] 0.49; ^{1}H NMR (500 MHz, $CDCl_3$): δ 0.83–0.90 (m, 3 H), 1.19 (d, *J* = 6.1 Hz, 3 H), 1.21–1.32 (m, 24 H), 1.32–1.46 (m, 2 H), 1.49–1.69 (m, 6 H), 2.24 (t, *J* = 7.6 Hz, 2 H), 3.56 (s, 3 H), 3.92–4.03 (m, 5 H), 4.88 (d, *J* = 6.6 Hz, 1 H), 7.49 (s, 1 H); ^{13}C NMR (126 MHz, $CDCl_3$): δ 14.2, 20.1, 22.8, 23.0, 25.2, 28.0, 29.3, 29.4, 29.5, 29.6, 29.7, 29.8 (6C), 32.0, 33.7, 34.9, 35.8, 41.3, 70.7, 107.8, 141.5, 148.9, 151.6, 155.4, 173.7; IR (nujol): ν_{max} = 3405, 1735, 1712, 1668, 1554, 1538; FTMS (ESI-TOF) *m/z*: $[M+H]^+$ Calcd for $C_{29}H_{51}N_4O_4^+$ *m/z*: 519.39048, Found 519.38994; GC [260 (const.)]: Not Found; UV/VIS: λ_{max} = 273 nm (EtOH); HPLC [*n*-hexane-2-PrOH (78:22, v/v); f = 1.0 mL/min; λ = 273 nm; *T* = 25 °C (Chiralpak AD-H)]: t_R=5.86 (*S*-isomer) and 7.06 min (*R*-isomer).

2.4. General procedure for the synthesis of racemic lisofylline levulinate (rac-3e)

To a solution of lisofylline (*rac*-**2**, 100 mg, 0.36 mmol), levulinic acid (83 mg, 0.72 mmol), and DMAP (15 mg) in CH_2Cl_2 (5 mL), EDCI hydrochloride (150 mg, 0.78 mmol) was added in one portion at 0–5 °C. Next, the reaction mixture was slowly warmed to room temperature and stirred for additional 48 h. After this time, content of the flask was diluted with CH_2Cl_2 (5 mL), washed with H_2O (4 × 10 mL), and the aqueous layer was back-extracted with CH_2Cl_2 (3 × 15 mL). The combined organic phases were washed again with H_2O (20 mL) and brine (20 mL), dried over anhydrous $MgSO_4$, filtered, and the permeate was concentrated *in vacuo*. The residue was purified by silica gel column chromatography using gradient of mixture of $CHCl_3$/MeOH (100:0, 98:2, 95:5, v/v) to provide the corresponding lisofylline levulinate (*rac*-**3e**, 53 mg, 0.14 mmol, 40 %) as a colorless oil. R_f [$CHCl_3$/MeOH (95:5, v/v)] 0.44; ^{1}H NMR (500 MHz, $CDCl_3$): δ 1.19 (d, *J* = 6.4 Hz, 3 H), 1.28–1.45 (m, 2 H), 1.49–1.57 (m, 1 H), 1.58–1.69 (m, 3 H), 2.17 (s, 3 H) 2.50–2.56 (m, 2 H), 2.72 (td, *J* = 6.6, 3.4 Hz, 2 H), 3.56 (s, 3 H), 3.94–4.02 (m, 5 H), 4.82–4.93 (m, 1 H), 7.49 (d, *J* = 0.5 Hz, 1 H); ^{13}C NMR (126 MHz, $CDCl_3$): δ 20.0, 22.9, 28.0, 28.5, 29.8, 30.0, 33.7, 35.7, 38.2, 41.3, 71.4, 107.8, 110.2, 141.5, 148.9, 151.6, 155.4, 172.5, 206.8; IR (nujol): ν_{max} = 3513, 3109, 2940, 2867, 1706, 1656, 1601, 1552, 1464, 1360, 1229, 1188, 1159, 1124, 1083, 1019, 978, 940, 847, 812, 764, 746, 656; FTMS (ESI-TOF) *m/z*: $[M+H]^+$ Calcd for $C_{18}H_{27}N_4O_5^+$ *m/z*: 379.19760, Found 379.19692; GC [260 (const.)]: t_R = 39.88 min; UV/VIS: λ_{max} = 274 nm (EtOH); HPLC [*n*-hexane-2-PrOH (78:22, v/v); f = 1.0 mL/min; λ = 273 nm; *T* = 25 °C (Chiralpak AD-H)]: t_R=22.98 (*S*-isomer) and 29.28 min (*R*-isomer).

2.5. General procedure for analytical-scale lipase-catalyzed KR of rac-2 – Enzyme screening

To a solution of racemic lisofylline (*rac*-**2**, 25 mg, 0.09 mmol) in $PhCH_3$ (2 mL) both vinyl acetate (959 mg, 11.15 mmol, 1 mL) and the respective enzyme preparation [25 mg, 100 %, w/w (catalyst/substrate *rac*-**2**)] were added at once. (Caution! Care must be taken to obtain homogenous solution of *rac*-**2** in $PhCH_3$; therefore, an intensive ultrasound irradiation of the suspension was conducted with additional heating of water bath at 50 °C for 15 min). The thus composed reaction mixture was stirred in thermo-stated glass vials ($V = 4$ mL) placed in anodized aluminum reaction block at 40 °C and 800 rpm for the time indicated in Table 1. The progress of EKR process was monitored by GC analysis for which the samples were prepared by withdrawing the suspension (50 μL) from the reaction mixture, dilution with a portion of CH_2Cl_2 (1 mL), and centrifugation of the enzyme using laboratory centrifuge (2 min, 6000 rpm). The enzymatic reaction was stopped by filtering off the enzyme under suction and rinsing the filtrate cake of exploited enzyme with $PhCH_3$ (2 mL). After evaporation of the volatiles from the permeate, the crude oil was subjected to SiO_2 column chromatography using gradient of $CHCl_3$/MeOH (98:2, 95:5 v/v) mixture yielding desired optically active (*S*)-(+)-**2** and (*R*)-(+)-**3a**.

2.6. General procedure for CAL-B-catalyzed KR of rac-2 – Kinetics of the EKR reactions

The reaction mixture composed of racemic lisofylline (*rac*-**2**, 25 mg, 0.09 mmol), $PhCH_3$ (2 mL), vinyl acetate (959 mg, 11.15 mmol, 1 mL) and the respective immobilized CAL-B biocatalyst [5 mg, 20 %, w/w (catalyst/substrate *rac*-**2**)] was stirred in thermo-stated sealed glass vial ($V = 4$ mL) placed in anodized aluminum reaction block at 40 °C and 800 rpm for the subsequent time-scale: 1 h, 1.5 h, 2 h, 2.5 h, 3 h and 3.5 h (for Novozym 435 and Lipozyme 435) or for 1 h, 2 h, 3 h, 4 h, 5 h and 8 h (for Chirazyme L-2, C-2 and Chirazyme L-2, C-3), respectively. Each of the enzymatic reaction was stopped by filtering off the enzyme on Schott funnel under vacuum, washing it with a portion of $PhCH_3$ (2 mL), and after evaporation of the volatiles from the filtrate, the crude oil was purified by column chromatography packed with a silica gel using gradient of $CHCl_3$/MeOH (98:2, 95:5 v/v) mixture as an eluent thus yielding desired optically active products (*S*)-(+)-**2** and (*R*)-(+)-**3a**. For additional data, see Table 2.

2.7. General procedure for (Chirazyme L-2, C-3)-catalyzed KR of rac-2 – Acyl donor screening

The reaction mixture containing racemic lisofylline (*rac*-**2**, 25 mg, 0.09 mmol), $PhCH_3$ (2 mL), the corresponding acylating agent (0.27 mmol, 3 equiv), and Chirazyme L-2, C-3 [5 mg, 20 % w/w (catalyst/substrate *rac*-**2**)] was stirred using a magnetic stirrer (800 rpm, IKA RCT basic) in thermo-stated sealed glass vial ($V = 4$ mL) at 40 °C for: 8 h [in the case of: vinyl acetate (23 mg, 25 μL), vinyl butyrate (31 mg, 33 μL), vinyl decanoate (53 mg, 61 μL) and vinyl palmitate (76 mg, 88 μL)] or 168 h [in case of: methyl levulinate (35 mg, 33 μL)], respectively. Further manipulations were carried out by analogy with the previous procedures for the enzyme screening, the investigations on the reaction kinetics and solvent screening. For additional data, see also Table 3.

2.8. General procedure for (Chirazyme L-2, C-3)-catalyzed KR of rac-2 – Solvent screening

The reaction mixture containing racemic lisofylline (*rac*-**2**, 25 mg, 0.09 mmol), the appropriate organic solvent (2 mL), vinyl acetate (23 mg, 0.27 mmol, 25 μL), and Chirazyme L-2, C-3 [5 mg, 20 % w/w (catalyst/substrate *rac*-**2**)] was stirred using a magnetic stirrer (800 rpm,

Table 1
Enzyme screening for enantioselective transesterification of *rac*-**2** under KR-conditions in $PhCH_3$.

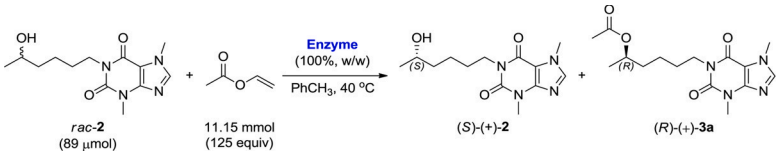

rac-**2** (89 μmol) | 11.15 mmol (125 equiv) | (*S*)-(+)-**2** | (*R*)-(+)-**3a**

Entry	Enzyme preparation[a]	*t* [h]	Conv.[b] [%]	ee_s[c] [%]/conf.[d]	ee_p[c] [%]/conf.[d]	*E*[e]
1	Novozym 435	5	53	>99/(*S*)	88/(*R*)	82
2	Lipozyme 435	5	54	>99/(*S*)	86/(*R*)	69
3	Chirazyme L-2, C-2	5	51	>99/(*S*)	95/(*R*)	>200
4	Chirazyme L-2, C-3	5	51	>99/(*S*)	96/(*R*)	>200
5	TL-Immobead 150	96	<10	N.D.[f]	N.D.[f]	N.D.f
6	Lipozyme TL IM	24	40	36/(*S*)	55/(*R*)	5
7	Lipozyme RM IM	96	<5	N.D.[f]	N.D.[f]	N.D.[f]
8	PS-Immobead 150	96	33	44/(*S*)	90/(*R*)	29
9	Amano PS-IM	5	42	69/(*S*)	95/(*R*)	81
10	Amano PS	96	46	75/(*S*)	87/(*R*)	32
11	Chirazyme L-10	5	58	93/(*S*)	68/(*R*)	17
12	Chirazyme L-5	24	63	76/(*S*)	44/(*R*)	6
13	Chirazyme L-8	144	27	21/(*S*)	58/(*R*)	5
14	Chirazyme L-3	144	31	11/(*R*)	24/(*S*)	2
15	Amano AK	96	52	77/(*S*)	72/(*R*)	14
16	Amano 10 Lipase M	96	<5	N.D.[f]	N.D.[f]	N.D.[f]
17	Amano M	96	<10	N.D.[f]	N.D.[f]	N.D.[f]
18	Amano Lipase F-AP15	96	<5	N.D.[f]	N.D.[f]	N.D.[f]
19	Lipase AY Amano 30	96	<10	N.D.[f]	N.D.[f]	N.D.[f]
20	PLE	96	<5	N.D.[f]	N.D.[f]	N.D.[f]

[a] Conditions: *rac*-**2** 25 mg, enzyme 25 mg, $PhCH_3$ 2 mL, vinyl acetate 959 mg, 1 mL (125 equiv), 40 °C, 800 rpm (magnetic stirrer).
[b] Based on GC, for confirmation the % conversion was calculated from the enantiomeric excess of the unreacted alcohol (ee_s) and the product (ee_p) according to the formula conv. = $ee_s/(ee_s + ee_p)$.
[c] Determined by chiral HPLC analysis by using a Chiralpak AD-H column.
[d] Absolute configuration.
[e] Calculated according to Chen et al. [82], using the equation: $E = \{\ln[(1 - \text{conv.})(1 - ee_s)]\}/\{\ln[(1 - \text{conv.})(1 + ee_s)]\}$.
[f] Not determined.

Table 2
Lipase screening for enantioselective transesterification of *rac*-**2** under KR-conditions in $PhCH_3$.

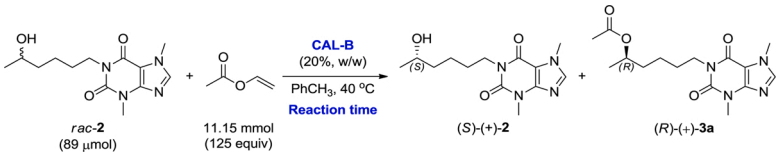

Entry	Lipase preparation[a]	*t* [h]	Conv.[b] [%]	ee_s[c] [%]	ee_p[c] [%]	*E*[d]
1	Novozym 435	1	28	38	99	>200
2		1.5	38	60	99	>200
3		2	43	74	99	>200
4		2.5	48	90	99	>200
5		3	48	91	98	>200
6		3.5	49	96	98	>200
7	Lipozyme 435	1	33	48	99	>200
8		1.5	37	58	99	>200
9		2	43	76	99	>200
10		2.5	47	87	98	>200
11		3	48	89	98	>200
12		3.5	48	91	98	>200
13	Chirazyme L-2, C-2	1	31	45	99	>200
14		2	39	64	99	>200
15		3	48	92	99	>200
16		4	49	94	99	>200
17		5	49	95	99	>200
18		8	50	>99	98	>200
19	Chirazyme L-2, C-3	1	32	47	>99	>200
20		2	42	71	>99	>200
21		3	48	90	>99	>200
22		4	48	93	>99	>200
23		5	50	98	99	>200
24		8	50	>99	99	>200

[a] Conditions: *rac*-**2** 25 mg, lipase 5 mg, $PhCH_3$ 2 mL, vinyl acetate 959 mg, 1 mL (124 equiv), 40 °C, 800 rpm (magnetic stirrer).
[b] Based on GC, for confirmation the % conversion was calculated from the enantiomeric excess of the unreacted alcohol (ee_s) and the product (ee_p) according to the formula conv. = $ee_s/(ee_s + ee_p)$.
[c] Determined by chiral HPLC analysis by using a Chiralpak AD-H column.
[d] Calculated according to Chen et al. [82], using the equation: $E = \{\ln[(1 - conv.)(1 - ee_s)]\}/\{\ln[(1 - conv.)(1 + ee_s)]\}$.

Table 3
Acyl donor screening for (Chirazyme L-2, C-3)-catalyzed KR of *rac*-**2** in $PhCH_3$ after 8–168 h.

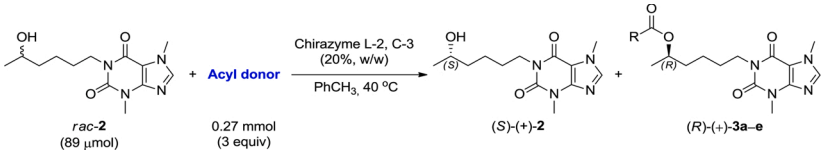

Entry	Acyl donor[a]	*t* [h]	Conv.[b] [%]	ee_s[c] [%]	ee_p[c] [%]	*E*[d]
1	Vinyl acetate (R = CH_3)	8	50	99	98	>200
2	Vinyl butyrate (R = C_3H_7)	8	53	99	88	82
3	Vinyl decanoate (R = C_9H_{19})	8	51	98	93	127
4	Vinyl palmitate (R = $C_{15}H_{31}$)	8	52	99	93	145
5	Methyl levulinate [R = $(CH_2)_2(CO)CH_3$]	168	32	46	>99	N.D.[e]

[a] Conditions: *rac*-**2** 25 mg, Chirazyme L-2, C-3 5 mg, $PhCH_3$ 2 mL, acyl donor (3 equiv), 40 °C, 800 rpm (magnetic stirrer).
[b] Calculated from the enantiomeric excess of the unreacted alcohol (ee_s) and the ester (ee_p) according to the formula conv. = $ee_s/(ee_s + ee_p)$.
[c] Determined by chiral HPLC analysis by using a Chiralpak AD-H column.
[d] Calculated according to Chen et al. [82], using the equation: $E = \{\ln[(1 - conv.)(1 - ee_s)]\}/\{\ln[(1 - conv.)(1 + ee_s)]\}$.
[e] Not determined. Since the reaction with methyl levulinate is not irreversible, hence the approximation cannot be used to calculate the *E*-value.

IKA RCT basic) in thermo-stated sealed glass vial ($V = 4$ mL) at 40 °C for 8 h. Further manipulations were carried out by analogy with the previous procedures for the enzyme screening and the investigations on the reaction kinetics. For additional data, see Table 4.

2.9. General procedure for (Chirazyme L-2, C-3)-catalyzed KR of rac-2 – Effect of temperature

The reaction mixture containing racemic lisofylline (*rac*-**2**, 25 mg, 0.09 mmol), EtOAc (2 mL), vinyl acetate (23 mg, 0.27 mmol, 25 μL), and Chirazyme L-2, C-3 [5 mg, 20 % w/w (catalyst/substrate *rac*-**2**)] was stirred (800 rpm, IKA RCT basic) in a thermo-stated sealed glass vial ($V = 4$ mL) for 3 h at 40 °C, 50 °C and 60 °C, respectively. After this time, the reaction was stopped by filtering off the enzyme on a Schott funnel under vacuum, washing it with a portion of EtOAc (2 mL), and after evaporation of the volatiles from the filtrate using a high-vacuum oil pump, the crude oil was transferred to an HPLC vial, re-dissolved in HPLC-grade 2-PrOH, and the samples were analyzed directly by HPLC equipped with chiral column. For additional data, see Table 5.

Table 4
Solvent screening for (Chirazyme L-2, C-3)-catalyzed KR of *rac*-**2** with vinyl acetate after 8 h.

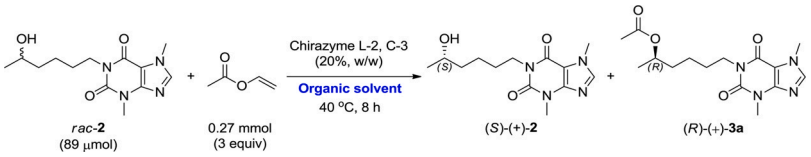

Entry	Solvent[a] (log *P*)[b]	Conv.[c] [%]	ee_s[d] [%]	ee_p[d] [%]	*E*[e]
1	1,4-Dioxane (-0.31)	49	96	99	>200
2	CH_3CN (0.17)	40	65	>99	>200
3	Acetone (0.20)	49	94	99	>200
4	EtOAc (0.29)	50	>99	99	>200
5	THF (0.40)	49	96	99	>200
6	Vinyl Acetate (0.54)	49	96	>99	>200
7	CH_2Cl_2 (1.01)	43	75	99	>200
8	*tert*-Amyl alcohol (1.09)	50	99	99	>200
9	$CHCl_3$ (1.67)	43	74	>99	>200
10	$PhCH_3$ (2.52)	50	>99	99	>200

[a] Conditions: *rac*-**2** 25 mg, Chirazyme L-2, C-3 5 mg, organic solvent 2 mL, vinyl acetate 23 mg, 25 μL (3 equiv), 40 °C, 800 rpm (magnetic stirrer).
[b] Logarithm of the partition coefficient of a given solvent between *n*-octanol and water according to ChemBioDraw Ultra 13.0 software indications.
[c] Based on GC, for confirmation the % conversion was calculated from the enantiomeric excess of the unreacted alcohol (ee_s) and the product (ee_p) according to the formula conv. = $ee_s/(ee_s + ee_p)$.
[d] Determined by chiral HPLC analysis by using a Chiralpak AD-H column.
[e] Calculated according to Chen et al. [82], using the equation: $E = \{\ln[(1 - conv.)(1 - ee_s)]\}/\{\ln[(1 - conv.)(1 + ee_s)]\}$.

Table 5
Temperature effect on (Chirazyme L-2, C-3)-catalyzed KR of *rac*-**2** with vinyl acetate in EtOAc after 3 h.

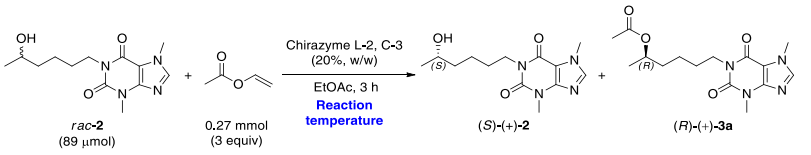

Entry	Temp.[a] (° C)	Conv.[b] [%]	ee_s[c] [%]	ee_p[c] [%]	*E*[d]
1	40	44	79	>99	>200
2	50	49	95	99	>200
3	60	50	97	99	>200

[a] Conditions: *rac*-**2** 25 mg, Chirazyme L-2, C-3 5 mg, EtOAc 2 mL, vinyl acetate 23 mg, 25 μL (3 equiv), 800 rpm (magnetic stirrer).
[b] Calculated from the enantiomeric excess of the unreacted alcohol (ee_s) and the acetate (ee_p) according to the formula conv. = $ee_s/(ee_s + ee_p)$.
[c] Determined by chiral HPLC analysis by using a Chiralpak AD-H column.
[d] Calculated according to Chen et al. [82], using the equation: $E = \{\ln[(1 - conv.)(1 - ee_s)]\}/\{\ln[(1 - conv.)(1 + ee_s)]\}$.

Table 6
Studies on the reaction time-course of the preparative-scale (Chirazyme L-2, C-3)-catalyzed KR of *rac*-**2** with vinyl acetate in EtOAc at 60 °C.

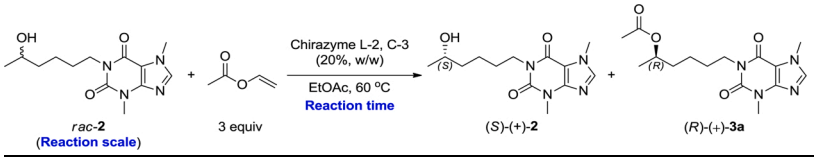

Entry	Scale	*t* [h]	Conv.[a] [%]	ee_s[b] [%]	ee_p[b] [%]	*E*[c]
1	250 mg[d]	1	47	89	99	>200
2		2	50	98	99	>200
3		3	50	99	98	>200
4		4	50	>99	98	>200
5	1.0 g[e]	1	47	89	99	>200
6		2	50	>99	>99	>200
7		3	50	99	98	>200
8		4	50	99	98	>200

[a] Based on GC, for confirmation the % conversion was calculated from the enantiomeric excess of the unreacted alcohol (ee_s) and the product (ee_p) according to the formula conv. = $ee_s/(ee_s + ee_p)$.
[b] Determined by chiral HPLC analysis by using a Chiralpak AD-H column.
[c] Calculated according to Chen et al. [82], using the equation: $E = \{\ln[(1 - conv.)(1 - ee_s)]\}/\{\ln[(1 - conv.)(1 + ee_s)]\}$.
[d] Conditions: *rac*-**2** 250 mg, Chirazyme L-2, C-3 50 mg, EtOAc 20 mL, vinyl acetate 230 mg, 250 μL (3 equiv), 800 rpm (magnetic stirrer).
[e] Conditions: *rac*-**2** 1 g, Chirazyme L-2, C-3 200 mg, EtOAc 80 mL, vinyl acetate 920 mg, 1 mL (3 equiv), 800 rpm (magnetic stirrer).

2.10. General procedure for (Chirazyme L-2, C-3)-catalyzed KR of rac-2 – 250 mg-scale

The reaction mixture containing racemic lisofylline (*rac*-**2**, 250 mg, 0.89 mmol), EtOAc (20 mL), vinyl acetate (230 mg, 2.68 mmol, 250 μL), and Chirazyme L-2, C-3 [50 mg, 20 % w/w (catalyst/substrate *rac*-**2**)] was stirred (800 rpm, IKA RCT basic, stirring bar: 2.0 cm, 3.38 g) in a tightly sealed round-bottomed flask ($V = 100$ mL) for 1 or 4 h at 60 °C, respectively. Next, the reaction was stopped by filtering off the enzyme on a Schott funnel under vacuum, washing it with a portion of EtOAc (20 mL), and after evaporation of the volatiles the crude oil was purified by silica gel column chromatography using gradient of mixture of $CHCl_3$/MeOH (98:2, 95:5, 90:10, 50:50 v/v) to provide the corresponding EKR products as follows: (*S*)-(+)-**2** (117 mg, 0.42 mmol, 47 %, 89 % ee for 1 h-reaction and 117 mg, 0.42 mmol, 47 %, 89 % ee for 4 h-reaction) and (*R*)-(+)-**3a** (130 mg, 0.40 mmol, 45 %, 99 % ee for 1 h-reaction and 144 mg, 0.45 mmol, 50 %, 98 % ee for 4 h- reaction). For additional data, see Tables 6 and 7.

2.11. General procedure for (Chirazyme L-2, C-3)-catalyzed KR of rac-2 – 1 g-scale

To a solution of racemic lisofylline (*rac*-**2**, 1 g, 3.57 mmol) in EtOAc (80 mL), vinyl acetate (920 mg, 10.70 mmol, 1 mL), and Chirazyme L-2, C-3 [200 mg, 20 % w/w (catalyst/substrate *rac*-**2**)] was stirred (800 rpm, IKA RCT basic; a stirring bar: 2.5 cm, 6.29 g) in a tightly sealed round-bottomed flask ($V = 250$ mL) for 2 or 4 h at 60 °C, respectively. After removal of the enzyme by filtration on a Schott funnel, washing it with portion of EtOAc (80 mL), and evaporation of the solvent under vacuum, the crude reaction mixture was purified by column chromatography on SiO_2 (ca. 55 g) using gradient of mixture of $CHCl_3$/MeOH (98:2, 95:5, 90:10, 50:50 v/v) as an eluent to afford the respective EKR products as follows: (*S*)-(+)-**2** (482 mg, 1.72 mmol, 48 %, 99 % ee for 2 h-reaction and 455 mg, 1.62 mmol, 46 %, >99 % ee for 4 h-reaction) and (*R*)-(+)-**3a** (546 mg, 1.69 mmol, 47 %, 97 % ee for 2 h-reaction and 540 mg, 1.68 mmol, 47 %, 97 % ee for 4 h-reaction). The results of specific rotation values for the EKR products are collected in Table S3 (see Supporting Information). For additional data, see Tables 6 and 7.

2.12. General procedure for analytical-scale lipase-catalyzed KR of rac-3a – Enzyme screening

Methanol (50 mg, 1.55 mmol, 63 μL) and the appropriate lipase [10 mg, 20 % w/w (catalyst/substrate)] were added to the solution of *rac*-**3a** (50 mg, 0.16 mmol) in CH_3CN (1 mL) and stirred (500 rpm) in a thermostated screw-capped test glass vial ($V = 4$ mL) at 25 °C for 48 h. Further manipulations were carried out by analogy with the previously described procedure for the enzyme screening (see section 2.2.); however, the EKR products were not purified by using column chromatography but analyzed directly as a crude reaction mixtures. For additional data, see Table 8.

2.13. Chemical K_2CO_3-mediated methanolysis of lisofylline acetate (R)-(+)-3a as the method for the synthesis of (R)-lisofylline [(R)-(−)-2]

To a solution of optically active lisofylline acetate [(*R*)-(+)-**3a**, 100 mg, 0.31 mmol, >99 % ee] in MeOH (10 mL) anhydrous K_2CO_3 (86 mg, 0.62 mmol) was added in one portion. The resulting mixture was stirred for 18 h at 22 °C. Next, the volatiles were evaporated under vacuum, and the crude oil was diluted with CH_2Cl_2 (10 mL) and rinsed with H_2O (2 × 10 mL). The combined organic phase was dried over anhydrous $MgSO_4$, the drying agent was filtered off, and the permeate was concentrated under vacuum. Finally, the remaining crude oil was subjected to a short-pad SiO_2 column chromatography and purified using gradient of mixture of $CHCl_3$/MeOH (98:2, 95:5 v/v) as an eluent yielding enantiomeric (*R*)-(–)-**2** (51 mg, 0.18 mmol, 59 %, 99 % ee) as colorless oil.

2.14. General procedure for the inversion of the absolute configuration in (S)-(+)-2 (see Step 1 and Step 2 below)

2.14.1. Step 1 {Synthesis of 6-(3,7-dimethyl-2,6-dioxo-2,3,6,7-tetrahydro-1H-purin-1-yl)hexan-2-yl methanesulfonate [(S)-(+)-4]}

To a stirred solution of optically active (*S*)-lisofylline [(*S*)-(+)-**2**, 100 mg, 0.36 mmol, >99 % ee] in dry CH_2Cl_2 (5 mL) cooled to 0–5 °C were added methanesulfonyl chloride (MsCl, 61 mg, 0.54 mmol, 41 μL) and Et_3N (54 mg, 0.54 mmol, 75 μL) in one portion. After 10 min of stirring the reaction mixture was warmed to room temperature and stirred for additional 1 h. Afterwards, the reaction mixture was diluted with CH_2Cl_2 (5 mL), and the organic phase was washed with saturated $NaHCO_3$ (3 × 10 mL), and back-extracted with CH_2Cl_2 (3 × 10 mL). The combined organic layer was quenched with brine (10 mL), dried over anhydrous $MgSO_4$, concentrated and the residue was purified by silica gel column chromatography using gradient of mixture of $CHCl_3$/MeOH (98:2, 95:5 v/v) as an eluent to afford corresponding optically active mesylate (*S*)-(+)-**4** {175 mg, 0.49 mmol, 68 %, 99 % ee, $[\alpha]_D^{26} = +3.5$ (*c* 1.00, $CHCl_3$)} as white solid. Mp 80–82 °C ($CHCl_3$/MeOH); R_f [$CHCl_3$/MeOH (95:5, v/v)] 0.60; ^{1}H NMR (500 MHz, $CDCl_3$): δ 1.41 (d, $J = 6.4$ Hz, 3 H) 1.43–1.55 (m, 2 H), 1.62–1.81 (m, 4 H), 2.99 (s, 3 H), 3.56 (s, 3 H), 3.91–4.07 (m, 5 H), 4.72–4.84 (m, 1 H), 7.50 (s, 1 H); ^{13}C NMR (126 MHz, $CDCl_3$): δ 21.4, 22.7, 27.7, 29.8, 33.7, 36.3, 38.7, 41.0, 80.2,

Table 7
Preparative-scale (Chirazyme L-2, C-3)-catalyzed KR of *rac*-**2** with vinyl acetate in EtOAc at 60 °C.

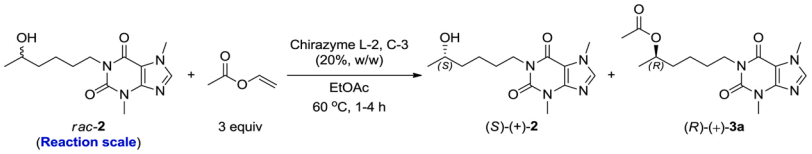

Entry	Scale	*t* [h]	Conv.[a] [%]	ee_s[b] [%]/Yield[c] [%]	ee_p[b] [%]/Yield[c] [%]	*E*[d]
1	250 mg[e]	1	47	89/47	99/45	>200
2		4	48	89/47	98/50	>200
3	1.0 g[f]	2	51	99/48	97/47	>200
4		4	51	>99/46	97/47	>200

[a] Based on GC, for confirmation the % conversion was calculated from the enantiomeric excess of the unreacted alcohol (ee_s) and the product (ee_p) according to the formula conv. = $ee_s/(ee_s + ee_p)$.
[b] Determined by chiral HPLC analysis by using a Chiralpak AD-H column.
[c] Isolated yield after column chromatography eluted with gradient of $CHCl_3$/MeOH (98:2, 95:5, 90:10, 50:50, v/v) mixture.
[d] Calculated according to Chen et al. [82], using the equation: $E = \{\ln[(1 - \text{conv.})(1 - ee_s)]\}/\{\ln[(1 - \text{conv.})(1 + ee_s)]\}$.
[e] Conditions: *rac*-**2** 250 mg, Chirazyme L-2, C-3 50 mg, EtOAc 20 mL, vinyl acetate 230 mg, 250 μL (3 equiv), 800 rpm (magnetic stirrer).
[f] Conditions: *rac*-**2** 1 g, Chirazyme L-2, C-3 200 mg, EtOAc 80 mL, vinyl acetate 920 mg, 1 mL (3 equiv), 800 rpm (magnetic stirrer).

Table 8
Enzyme screening for enantioselective methanolysis of *rac*-**3a** under KR-conditions in CH_3CN.

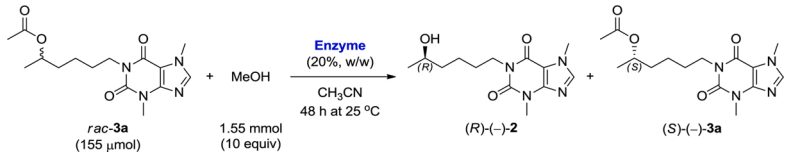

Entry	Enzyme preparation[a]	Conv.[b] [%]	ee_s[c] [%]/conf.[d]	ee_p[c] [%]/conf.[d]	E[e]
1	Novozym 435	37	58/(*S*)	>99/(*R*)	>200
2	Lipozyme 435	42	72/(*S*)	>99/(*R*)	>200
3	Chirazyme L-2, C-2	32	46/(*S*)	>99/(*R*)	>200
4	Chirazyme L-2, C-3	28	38/(*S*)	>99/(*R*)	>200
5	TL-Immobead 150	0	N.D.[f]	N.D.[f]	N.D.[f]
6	Lipozyme TL IM	<5	N.D.[f]	N.D.[f]	N.D.[f]
7	Lipozyme RM IM	<5	N.D.[f]	N.D.[f]	N.D.[f]
8	PS-Immobead 150	0	N.D.[f]	N.D.[f]	N.D.[f]
9	Amano PS-IM	<5	N.D.[f]	N.D.[f]	N.D.[f]
10	Amano PS	<5	N.D.[f]	N.D.[f]	N.D.[f]
11	Chirazyme L-10	<5	N.D.[f]	N.D.[f]	N.D.[f]
12	Chirazyme L-5	0	N.D.[f]	N.D.[f]	N.D.[f]
13	Chirazyme L-8	<5	N.D.[f]	N.D.[f]	N.D.[f]
14	Chirazyme L-3	0	N.D.[f]	N.D.[f]	N.D.[f]
15	Amano AK	0	N.D.[f]	N.D.[f]	N.D.[f]
16	Amano 10 Lipase M	0	N.D.[f]	N.D.[f]	N.D.[f]
17	Amano M	0	N.D.[f]	N.D.[f]	N.D.[f]
18	Amano Lipase F-AP15	0	N.D.[f]	N.D.[f]	N.D.[f]
19	Lipase AY Amano 30	<5	N.D.[f]	N.D.[f]	N.D.[f]
20	PLE	0	N.D.[f]	N.D.[f]	N.D.[f]

[a] Conditions: *rac*-**3a** 50 mg, enzyme 10 mg, CH_3CN 1 mL, MeOH 50 mg, 63 μL (10 equiv), 25 °C, 500 rpm (magnetic stirrer).
[b] Based on GC, for confirmation the % conversion was calculated from the enantiomeric excess of the unreacted ester (ee_s) and the product (ee_p) according to the formula conv. = $ee_s/(ee_s + ee_p)$.
[c] Determined by chiral HPLC analysis by using a Chiralpak AD-H column.
[d] Absolute configuration.
[e] Calculated according to Chen et al. [82], using the equation: $E = \{\ln[(1 - conv.)(1 - ee_s)]\}/\{\ln[(1 - conv.)(1 + ee_s)]\}$.
[f] Not determined.

107.8, 141.6, 148.9, 151.6, 155.4; IR (nujol): ν_{max} = 3437, 1694, 1660, 1544, 1452, 1176, 978, 912, 761; HRMS (ESI-TOF) *m/z*: $[M+H]^+$ Calcd for $C_{14}H_{23}N_4O_5S^+$ *m/z*: 359.1384, Found 359.1380; GC [260 (const.)]: t_R = 12.35 min; UV/VIS: λ_{max} = 207 nm (EtOH); HPLC [*n*-hexane-2-PrOH (78:22, v/v); f = 1.0 mL/min; λ = 273 nm; *T* = 25 °C (Chiralpak AD-H)]: t_R=33.937 (*S*-isomer) and 49.346 min (*R*-isomer).

2.14.2. Step 2 [Synthesis of (R)-(+)-3a from methanesulfonate (S)-(+)-4]

To a solution of mesylate (*S*)-(+)-**4** (10 mg, 27.9 μmol) in dry $PhCH_3$ (2 mL) CsOAc (11 mg, 55.8 μmol) and catalytic amount of 18-Crown-6 (5 mg) were added in one portion. The reaction mixture was stirred for 18 h at 110 °C, and afterwards poured into H_2O (5 mL) and extracted with EtOAc (3 × 2 mL). The collected organic phases were dried over anhydrous $MgSO_4$ and after evaporation of the volatiles under reduced pressure the crude product was purified by column chromatography on silica gel using pure EtOAc as an eluent to afford optically active acetate (*R*)-(+)-**3a** (4.5 mg, 14 μmol, 50 %, 96 % ee) as white solid. All the analyses were consistent with *rac*-**3a**.

2.15. XRD analyses

2.15.1. Conditions for crystal growth of (S)-lisofylline [(S)-(+)-2] and (R)-lisofylline [(R)-(–)-2]

Colorless single crystal of sufficient quality for a structure analysis with conventional X-ray diffraction (XRD) method was prepared by dissolving (*S*)-(+)-**2** (30 mg, >99 % ee) in boiling EtOAc (2 mL). After refluxing the content of the flask for additional 2–3 min, the hot solution was slightly cooled, then transferred into open-neck glass vial (*V* = 4 mL), closed with the cap, left to cool to room temperature, then opened and placed in a larger bottle that contained hexane. The outer vessel was sealed, and thus composed system was stored at room temperature, and crystal growth was proceeded for 2 days by slow vapor diffusion of the precipitant (hexane) into saturated EtOAc solution of (*S*)-(+)-**2**. The monocrystals of (*R*)-(–)-**2** were grown exactly in the same manner as for its counterpart (*S*)-(+)-**2**.

2.15.2. Crystal structure determination

Selected crystals were measured with mirror monochromated CuK_α radiation on an Oxford Diffraction κ-CCD Gemini A Ultra diffractometer. Cell refinement and data collection as well as data reduction and analysis were performed with the Rigaku Oxford CRYSALIS^{PRO} software. Using Olex2 [37], the structure was solved with the ShelXT [38] structure solution program using Intrinsic Phasing and refined with the ShelXL [39] refinement package using Least Squares minimisation. All non-hydrogen atoms were refined with anisotropic displacement parameters. Hydrogen atoms attached to carbon atoms were added to the structure model at geometrically idealized coordinates and refined as riding atoms. An absolute configuration for the molecules were successfully determined using anomalous dispersion effects. Flack parameters were calculated from selected quotients (Parsons' method) [40]. Further analysis of the absolute structure was performed using likelihood methods with PLATON [41] using Bijvoet pairs to obtain the Hooft parameters [42]. CCDC 2023424-2023425 contains the supplementary crystallographic data for both enantiomeric compounds (*S*)-(+)-**2** and (*R*)-(–)-**2**. This can be obtained free of charge on application to CDC, 12 Union Road, Cambridge CB21EZ, UK (Fax: (+44)1223-336-033; email: deposit@ccdc.cam.ac.uk).

2.15.2.1. Crystal data for (S)-(+)-2. $C_{13}H_{20}N_4O_3$ (*M* = 280.33 g/mol): monoclinic, space group $P2_1$ (no. 4), *a* = 10.1581(2) Å, *b* = 13.1633(2) Å, *c* = 11.6783(2) Å, *β* = 112.436(2)°, *V* = 1443.35(5) Å^3, *Z* = 4, *T* = 293.15 K, $\mu(CuK_\alpha)$ = 0.772 mm^{-1}, crystal size = 0.438 × 0.305 × 0.242 mm^3, *Dcalc* = 1.290 g/cm^3, 71,878 reflections measured (8.19° ≤ 2Θ ≤ 134.134°), 5140 unique (R_{int} = 0.0524, R_{sigma} = 0.0163) which were

used in all calculations. The final R_1 was 0.0430 ($I > 2\sigma(I)$) and wR_2 was 0.1134 (all data), *GoF* = 1.045, largest diff. peak/hole = 0.13/-0.17/ e·Å^{-3}, Flack parameter = 0.01(15), Hooft parameter = 0.05(12) from 2446 pairs (100 % coverage).

2.15.2.2. Crystal data for (r)-(–)-2. $C_{13}H_{20}N_4O_3$ (M = 280.33 g/mol): monoclinic, space group $P2_1$ (no. 4), a = 10.1566(2) Å, b = 13.1561(2) Å, c = 11.6737(2) Å, β = 112.441(2)°, V = 1441.73(5) Å^3, Z = 4, T = 293.15 K, $\mu(CuK_\alpha)$ = 0.773 mm^{-1}, crystal size = 0.461 × 0.344 × 0.327 mm^3, *Dcalc* = 1.291 g/cm^3, 39,430 reflections measured (8.194° ≤ 2Θ ≤ 134.134°), 5129 unique (R_{int} = 0.0742, R_{sigma} = 0.0306) which were used in all calculations. The final R_1 was 0.0422 ($I > 2\sigma(I)$) and wR_2 was 0.1204 (all data), *GoF* = 1.037, largest diff. peak/hole = 0.18/-0.16/ e·Å^{-3}, Flack parameter = 0.01(12), Hooft parameter = 0.03(10) from 2437 pairs (100 % coverage).

2.16. Molecular docking experiments

Molecular docking studies to establish favorable ligand binding geometries for both enantiomers of 1-(5-hydroxyhexyl)-3,7-dimethyl-3,7-dihydro-1*H*-purine-2,6-dione [(*S*)-(+)-**2** and (*R*)-(–)-**2**] were carried out on a 4 CPUs-based desktop PC computer equipped with AMD Phenom™ II X4 965 Processor 3.40 GHz and 32 GB of RAM on a Microsoft Windows 10 Professional 64-bit operating system using AutoDock Vina vs. 1.1.2 program for Windows (http://autodock.scripps.edu/) [43]. The respective ligand molecules (*S*)-(+)-**2** and (*R*)-(–)-**2** were prepared at first with ChemAxon MarvinSketch vs. 14.9.1.0 (http://www.chemaxon.com/marvin/) using general 'Cleaning in 3D' option and calculating conformers with MMFF94 force field parameters. To obtain the minimum energy conformation for docking studies, the geometries of the afore-pretreated ligands were additionally optimized in Avogadro version 1.2.0. (http://avogadro.cc/), after adding all the hydrogens, and saved as mol2 files. The minimum energies were obtained for each ligand: (*S*)-(+)-**2** ($E_{calc.}$ = –491.888 kJ/mol) and (*R*)-(–)-**2** ($E_{calc.}$ = –491.567 kJ/mol). The visualization of the optimized geometries were performed using molecular visualization software, POV-Ray for Windows v3.7.0.msvc10.win64 licensed under the terms of the GNU Affero General Public License (AGPL3) (Fig. 2). The Gasteiger partial charges were calculated with AutoDock Tools vs. 1.5.6 (ADT, S3 http://mgltools.scripps.edu/) [44], whereas all torsion angles for each enantiomer of **2** were considered flexible, and all the possible rotatable bonds, non-polar hydrogens were determined, and the final ligands' files were prepared in PDBQT format, respectively.

The crystallographic structure of lipase type B from *Candida antarctica* (PDB code: 1TCA) [45] were downloaded from Brookhaven RCSB Protein Data Bank (PDB, http://www.rcsb.org/pdb/). To avoid steric clashes within model the crude protein. pdb file was prepared by UCSF Chimera vs. 1.11.2 package (http://www.cgl.ucsf.edu/chimera/) [46] by removing all nonstandard (non-protein) molecules including conserved crystal waters (HOH) and *N*-acetyl-D-glucosamine (NAG), respectively. The polar hydrogen atoms were added and Gasteiger charges were calculated with AutoDock Tools 1.5.6 package using its standard utility scripts, and then the final protein file was saved as PDBQT file. Next, a searching 'grid box' was set by using AutoGrid function to perform docking in a (40 × 40 × 40 Å)-unit grid box, centered on catalytic Ser105 of CAL-B as target coordinate (center_x = −3.144; center_y = 21.093; center_z = 12.736) with a grid spacing of 0.325 Å. In addition, construction of the acetyl-lipase structure (with modified side chain hydroxyl group of the Ser105 of CAL-B) was prepared by standard 'Build' options available in Maestro Schrödinger Version 12.6.144, MMshare Version 5.2.144, Release 2020−4, Platform Windows-x64 (https://www.schrodinger.com/maestro). Then, the energy of this system was further minimized by executing 1000 Conjugate Gradient steps, with a fix constraint applied to the protein backbone.

Docking was performed into a rigid protein as well as using advanced protein flexibility by specifying flexible sidechains. Each docking was performed with an exhaustiveness level of 48. For each ligand molecule 100 independent runs were performed using the Lamarckian Genetic Algorithm (GA) with at most 106 energy evaluations and a maximum number of generations of >27 000 Å^3 (the search space volume). The rest of the docking parameters including the remaining Lamarckian GA parameters were set as default using the standard values for genetic Vina algorithms (the posed dockings were below 5.00 Å rmsd). The docking modes of each ligand (*S*)-(+)-**2** and (*R*)-(–)-**2** were clustered and ranked based on a mutual ligand–protein affinity expressed as absolute free binding energies [ΔG_{calc} (kcal/mol)] as well as the values of root mean square deviation (rmsd) in both modes regarding rmsd lower bound (l. b.), and rmsd upper bound (u.b.), respectively. The rmsd were computed referring to the input structure submitted to docking simulations. For (*S*)-(+)-**2** the used random seed amounted to 1962309292, whereas for (*R*)-(–)-**2**: 447232740. The results generated by AutoDock Vina including optimized binding poses of substrates (*S*)-(+)-**2** and (*R*)-(–)-**2** in both hypothetical CAL-B-enantiomers' complexes as well as critical polar contacts between the respective atoms of ligands (*S*)-(+)-**2** and (*R*)-(–)-**2** and receptor molecule (CAL-B, 1TCA) were visualized using The PyMOL Molecular Graphics System software, version 1.3, Schrödinger, LLC (https://www.pymol.org/).

3. Results and discussion

Herein, we report on devising enantioselective and stereoconvergent route toward enantiomeric (*R*)-lisofylline [(*R*)-(–)-**2**]. In this regard, the synthetic pathway of chemoenzymatic asymmetric preparation of non-racemic title API consisting of a classical enzymatic kinetic resolution (EKR) methodology as a key-step is outlined in Scheme 1.

We decided to choose lipases as the biocatalysts for routine EKR of *rac*-**2** since these enzymes, although considered as 'old-fashioned', still remain unsurpassed in specificity and scope of action, which features are especially useful in pharmaceutical applications [47–51]. The major

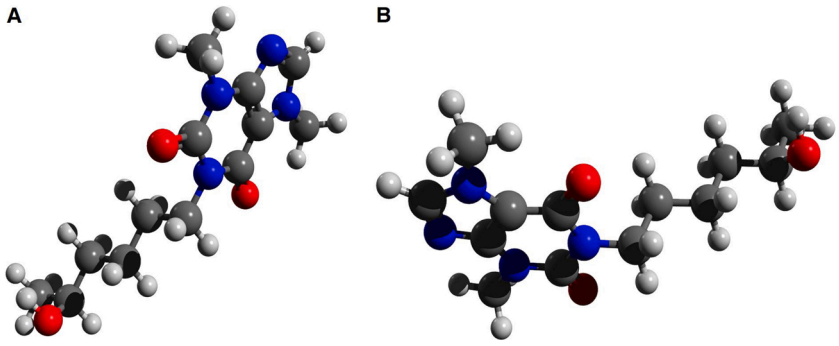

Fig. 2. The geometries of (*S*)-(+)-**2** (**A**) and (*R*)-(–)-**2** (**B**) optimized in Avogadro – Version 1.2.0. The figures were prepared by rendering them by using molecular visualization software, POV-Ray – Version 3.7.0.

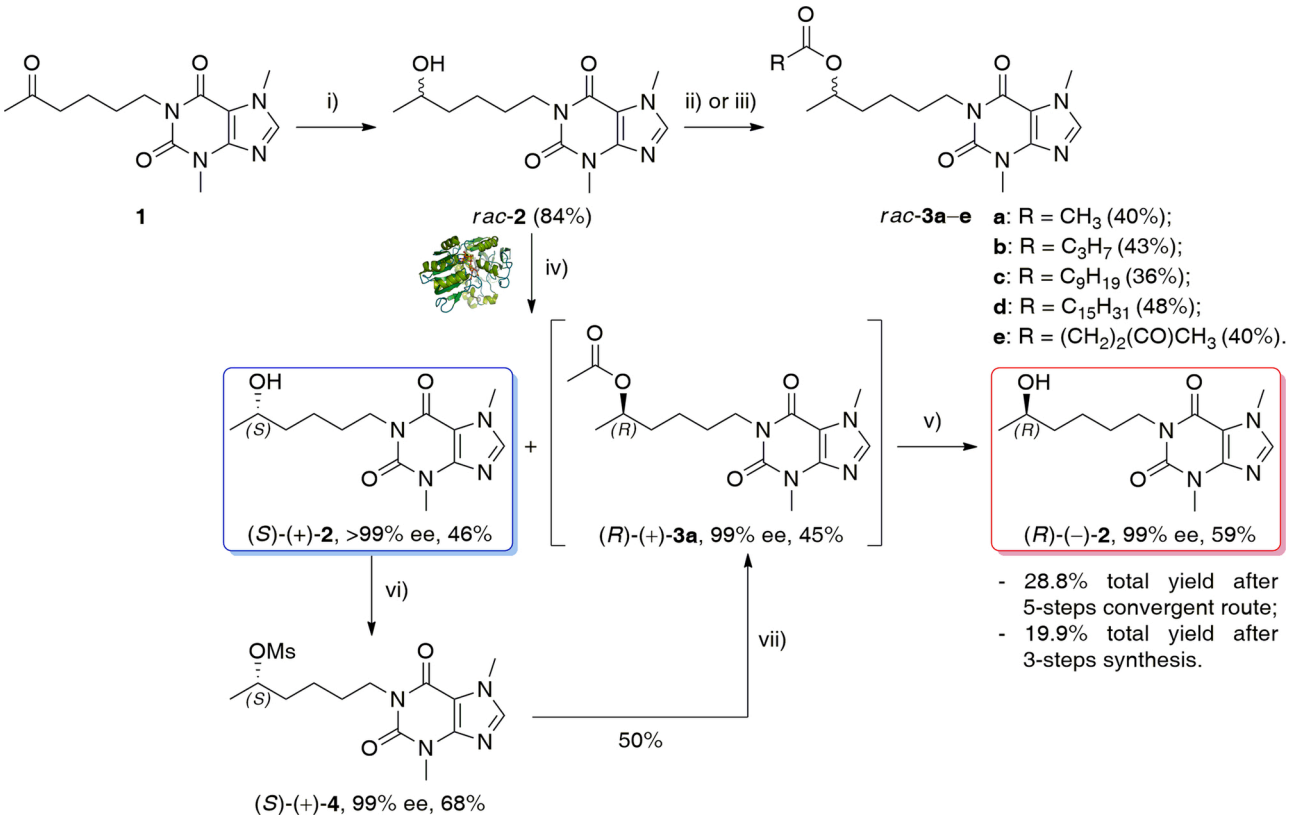

Scheme 1. Chemoenzymatic synthesis of lisofylline enantiomers (**2**). Reagents and conditions: (i) $NaBH_4$ (3 equiv), MeOH/CH_2Cl_2 (40:6, v/v), 2.5 h at 0–5 °C; (ii) acetyl chloride (1.5 equiv), Et_3N (1.5 equiv), DMAP (cat.), dry CH_2Cl_2, 10 min at 0–5 °C, then 12 h at RT; (iii) levulinic acid (2 equiv), EDCI hydrochloride (2.2 equiv), DMAP (cat.), dry CH_2Cl_2, 10 min at 0–5 °C, then 48 h at RT; (iv) vinyl acetate (3.0 equiv), Chirazyme L-2, C-3 (20 % w/w), EtOAc (80 mL/1 g of substrate), 1–4 h at 60 °C, 800 rpm (magnetic stirrer); (v) K_2CO_3 anh. (2 equiv), MeOH, 18 h at 22 °C; (vi) MsCl (1.5 equiv), Et_3N (1.5 equiv), dry CH_2Cl_2, 10 min at 0–5 °C 10 min, then 1 h at RT; (vii) CsOAc (2 equiv), dry $PhCH_3$, 18-Crown-6 (cat.), 18 h at 110 °C.

advantages of using lipases, aside their ability to transform a plethora of diverse xenobiotics provided with mostly high chemo-, regio-, and stereo-selectivity under mild reaction conditions (pH 5–8, 20–40 °C, standard pressure) [52], are their low cost, great operational stability and ease of handling. Immense potential of using lipases also stems from a very distinct feature, namely that they remain catalytically active without a need for costly external acceptors and cofactors [i.e. NAD(P)H, $FADH_2$ etc.] present in the reaction system, and what is even more important, that they are able to catalyze reactions under non-physiological conditions in nearly non-aqueous media, including organic solvents [53,54], neoteric solvents [i.e. ionic liquids (ILs), supercritical carbon dioxide ($scCO_2$), fluorous solvents (FSs), and liquid polymers (LPs)] [55–58], deep eutectic solvents (DESs) [59–62] as well as in solvent-free systems [63–66] or even under mechanochemical conditions [67,68]. The great organic solvent tolerance of lipases (predestining them to perform with high concentrations of water-insoluble substrates) together with adaptability to various technological conditions without necessity to follow the restrictions imposed on metal-based catalysts make these enzymes willingly applied by industry [69]. In addition, tailoring and optimizing catalytic functions of lipases via enzyme engineering is becoming faster and more efficient [70–73].

Moreover, development of a highly efficient gram-scale EKR synthetic strategy to access lisofylline in both enantiomeric forms is critical for exploring their structure–activity relationships (SAR) and assisting further pharmacological studies for better understanding of their biological effects and potential mechanisms of action at the molecular level.

3.1. Synthesis of Racemic Compounds rac-2 and rac-3a–e

Our synthesis commenced with the preparation of racemic substrate *rac*-**2** and the reference esters *rac*-**3a–e** required for biocatalytic studies and analytical purposes. This task was achieved using standard synthetic methodology starting with the corresponding commercially available pentoxifylline (**1**, 3,7-dimethyl-1-(5-oxohexyl)-3,7-dihydro-1*H*-purine-2,6-dione). In the first step, racemic lisofylline (*rac*-**2**) was prepared following a slightly modified literature procedure reported by Peterson et al. [9]. For this purpose, prochiral ketone **1** was subjected to a non-selective chemical reduction with 3 equiv of sodium borohydride ($NaBH_4$) as the reducing agent suspended in a cold mixture of MeOH/CH_2Cl_2 (46 mL; 40:6, v/v). The reaction proceeded smoothly and was completed in a 2.5-h time span, thus affording *rac*-**2** in high 84 % yield after recrystallization. Next, the respective racemic esters *rac*-**3a–d** were obtained through a simple esterification procedure of catalysis by *N*,*N*-dimethylpyridin-4-amine (DMAP) using 1.5 equiv of the appropriate acyl chloride in the presence of 1.5 equiv of triethylamine (Et_3N) in dry CH_2Cl_2. In turn, racemic levulinate *rac*-**3e** was synthesized by the treatment of *rac*-**2** with 2 equiv. of levulinic acid in the presence of 2.2 equiv. of 1-ethyl-3-(3-dimethylaminopropyl)carbodiimide hydrochloride (EDC×HCl) as the coupling reagent and a catalytic amount of DMAP diluted in anhydrous CH_2Cl_2 at ambient temperature. The above-mentioned acylations of *rac*-**2** led to obtaining desired esters *rac*-**3a–e** in a 36–48 % yield range, respectively (Scheme 1).

Next, with the racemic compounds in hand *rac*-**2** and *rac*-**3a–e**, the HPLC separation conditions of the respective enantiomers were established. Fortunately, the chromatographic base-line resolutions of the enantiomers of all the examined racemates *rac*-**2** and *rac*-**3a–e** were achieved within a suitable time using only one HPLC column packed with amylose-type chiral stationary phase (Chiralpak AD-H) and a single analytical method (Supporting Information). This allowed to investigate the stereoselectivity of the biocatalytic reactions involving racemic

lisofylline (*rac*-**2**) in a relatively rapid way without any analytical obstruction.

3.2. Lipase-catalyzed KR of racemic lisofylline (rac-2)

At the outset of biocatalytic investigations our major task was to find an enzyme with reasonable catalytic activity and high enantioselectivity in kinetic resolution of racemic lisofylline (*rac*-**2**). Taking an advantage of our experience in the field of enzyme catalysis [74,75] and especially the expertise in the chemoenzymatic syntheses of various chiral APIs [76,77] including proxyphylline enantiomers [78] as well as enantiomerically enriched diprophylline and xanthinol nicotinate [79], we turned our attention to studying the lipase-catalyzed enantioselective transesterification of racemic lisofylline (*rac*-**2**) using vinyl acetate (VA) as an acetyl donor in neat organic solvents. This methodology is highly preferable from the industrial point of view since 'irreversible-acetylation mode' assured by activated enol esters does not hinder the isolation and purification process as liquid-liquid extraction workup is redundant and the volatile by-products are easily removable under reduced pressure, whilst the insoluble enzyme can be simply filtered off under suction [80,81].

For this reason, the analytical-scale enantioselective lipase-catalyzed acetylation of *rac*-**2** was firstly investigated using a huge excess of vinyl acetate (1 mL, 125 equiv) and a set of 19 various native and/or immobilized commercial lipases as well as single esterase from porcine liver (Table 1). The EKR of *rac*-**2** were carried out in the presence of 100 % (w/w) loading of the respective enzyme preparation with respect to the employed substrate *rac*-**2** in toluene ($PhCH_3$) as a model co-solvent. The enzymatic reactions were stirred at 40 °C, regularly traced by GC analysis and terminated either upon achieving 50 % conv., or in case of the less active enzymes, until 144 h had passed. The conversion and the enantiomeric excesses of the chromatographically purified EKR products were measured by HPLC on a chiral phase. The enzyme screening showed that most of the tested biocatalysts exhibited low enantioselectivities (E = 2–82) and activities or were active in a non-selective manner. The best results were obtained only with lipases B from *Candida antarctica* (CAL-B), which catalyzed EKR of *rac*-**2** with 51–54 % conv. after 5 h (Table 1, entries 1–4). Interestingly, among CAL-B preparations two of them, namely Novozym 435 and Lipozyme 435, catalyzed acetylation of the racemic lisofylline (*rac*-**2**) with moderate enantioselectivity (E = 69–82), while both Chirazyme L-2, C-2 and Chirazyme L-2, C-3 proved to be significantly more efficient in the resolution of *rac*-**2** enantiomers (E>200) providing homochiral unreacted (*S*)-(+)-**2** (>99 % ee) and enantiomerically-enriched acetate (*R*)-(+)-**3a** in a 95–96 % ee range with E>200, respectively.

These results clearly indicate that for desired catalytic behavior of biocatalysts not only the enzymes' origin (source) is critical, but even negligible differences in the utility form. As in the example, the method of immobilization and/or the type of the enzyme's carrier might affect functions of particular preparations isolated from the same microorganism. Almost all the enzymatic reactions followed the empirical rule proposed by Kazlauskas [83] and in each case, the (*R*)-enantiomer was acylated faster by the enzymes. Surprisingly, after detailed examination of the performed EKR attempts one native lipase from *Candida rugosa* (Chirazyme L-3) revealed reversed (*S*)-stereopreferance toward *rac*-**2** (Table 1, entry 14). Nevertheless, this unique 'anti-Kazlauskas' type lipase preparation was omitted in further studies since it catalyzed the KR of *rac*-**2** very sluggishly and without promising enantioselectivity.

Taking into account that a single random EKR result would have been insufficient to select a suitable biocatalyst for efficient EKR as well as the fact that preliminary experiments showed that the highest catalytic activity and enantioselectivity discrimination during the transesterification of *rac*-**2** was observed in the case of *C. albicans* lipases B, in the next step of optimization studies a comprehensive kinetic analyses were assessed for all CAL-B preparations (Table 2). The evaluation of the effect of the reaction time on the conversion degree of *rac*-**2** would provide a better insight into the reaction progress as well as a stereochemical outcome of the overall process. The EKR's assays were arbitrarily terminated at periodic time intervals adjusted to the respective enzyme and its activity. Since the rates of both (Novozym 435)- and (Lipozyme 435)-catalyzed reactions were slightly higher when compared with Chirazymes-mediated processes, the EKR progress in those cases was assessed in 1–3.5 h time span within more frequent 30 min. intervals, respectively. After isolation and subsequent chromatographic purification of the resolution products the evaluation of their enantiomeric excesses (% ee) as well as the reactions' E-values was made.

From a series of kinetic experiments data, it was concluded that the most outstanding results in terms of enantioselectivity toward lisofylline (*rac*-**2**) enantiomers was shown by Chirazyme L-2, C-3, which allowed to obtain both optically pure EKR products (*S*)-(+)-**2** and (*R*)-(+)-**3a** depending on the moment of terminating the reaction. In turn, CAL-B immobilized on acrylic resins (Novozym 435 and Lipozyme 435) transpired to catalyze *rac*-**2** enantiomers resolution with mostly excellent enantioselectivity (E>200) resulting in the formation of almost enantiomerically pure acetate (*R*)-(+)-**3a** (99 % ee). Nevertheless, the remaining slower-reacting enantiomer (*S*)-(+)-**2** barely reached 96 % ee. Elongation of the time of EKR would definitely lead to more optically pure (*S*)-(+)-**2** as had been shown in previous experiments (Table 1), although this came at the expense of the purity of the second enantiomer (*R*)-(+)-**3a**. As it was clear that proceeding the EKR of *rac*-**2** with Chirazyme L-2, C-3 as the biocatalyst for 8 h allowed to afford superb enantioselectivity (E>200) leading to isolation of enantiomerically pure stereoisomers (*S*)-(+)-**2** and (*R*)-(+)-**3a** (99–99.9 % ee), the subsequent optimization steps were conducted using this biocatalytic system.

Another variable parameter, which exerts a significant impact on the rate and enantioselectivity of enzymatic reactions is the type of the acyl donor. Since i.e. triglycerides (TAGs), cholesteryl esters and/or wax esters constitute the major physiological substrates of the lipases *in vivo*, it is rather obvious that these hydrolytic enzymes show preference toward acyl donors, which possess long-chain fatty acids in their structures. The conversion of alcohol mostly improves on increase in the acid chain length. This is probably because of the interfacial activation of lipases is more efficient in the presence of more hydrophobic compounds and/or the hydrophobic pocket of the binding site (so-called 'acyl site') stabilizes better the longer acyl chains [84–87]. As a matter of fact, *Candida antarctica* lipase B behaves more like a solvent-stable esterase and does not display interfacial activation due to the absence of a lid that regulates the access to the active site [88]. Nevertheless, the enantioselectivity of CAL-B can also be strongly influenced by the chain length of the achiral acyl donor employed in the transesterification [89]. Hence, the influence of the nature of acyl donor on the course of the lisofylline (*rac*-**2**) acylation was examined using 4 different vinyl esters with various chain lengths and one alkyl ester possessing terminal methyl ketone moiety (Table 3). Furthermore, to minimize the costs of the overall enzymatic process the reduction of biocatalyst loading (from 100 % to 20 % w/w in respect to *rac*-**2**) as well as the decrease in the molar excess of the appropriate acyl donor reagent (from 125 equiv to 3 equiv) were investigated under optimal EKR conditions. Moreover, the reduction in amounts of the employed vinyl acetate at this stage seems to be reasonable since this compound generates very toxic, irritating, highly volatile, flammable and explosive acetaldehyde. Moreover, acetaldehyde is responsible for enzyme inhibition due to formation of stable Schiff base-type adducts with the side chain –NH group of peripheral lysine residues [90,91], while the synthesis of vinyl acetate is hazardous in fact. Therefore, eliminating the need of using huge molar excess of vinyl acetate as well as other acylating agents should allow to safely scale-up the reaction.

Consideration of the results summarized in Table 3 leads to the conclusion that the highest enantioselectivity (E>200) was observed in the transesterification of *rac*-**2** with vinyl acetate as an acyl donor. When the reaction was arbitrarily arrested after 8 h, the optically active

lisofylline acetate (*R*)-(+)-**3a** was isolated in very high enantiomeric purity (98 % ee) leaving thereby slower reacting stereoisomer (*S*)-(+)-**2** in homochiral form (>99 % ee). To our disappointment, no impressive enhancement of the catalytic activity and stereoselectivity of Chirazyme L-2, C-3 lipase in the presence of fatty acids vinyl esters were observed since the reaction rates were almost the same reaching approx. 50 % conv. The biotransformations of *rac*-**2** using vinyl esters with longer aliphatic chains (i.e. vinyl decanoate and vinyl palmitate) akin to acid moiety present in typical natural lipases' substrates were slightly improved in terms of *E*-values compared to vinyl butyrate, but worse than those conducted with vinyl acetate and methyl levulinate, respectively. In turn, the EKR of *rac*-**2** carried out with methyl levulinate required a substantially longer reaction time (168 h) to achieve reasonable conversions (Table 3, entry 5). The sluggish reactivity of *rac*-**2** with methyl levulinate might be 2-fold: additional methyl ketone moiety interacts with nucleophilic amino-acid residues present in the CAL-B active site thus affecting the enzymatic activity and/or unfavorable equilibrium of the (*R*)-(+)-**3e** formation due to reversible nature of the acyl donor and possible inhibition by the released methanol. To drive this reaction to 50 % completion, removal of the forming alcohol by evaporation, azeotropic distillation and/or addition of molecular sieves is necessary.

The conversion of acylation of *rac*-**2** using vinyl acetate was slightly retarded when compared to fatty acid acyl donors as evidenced by GC and HPLC analyses. However, it can be seen that reduction in the lipase loading and acyl transfer reagent concentration did not decrease the rate of the reaction at all. Moreover, vinyl acetate is much less expensive than the rest of the employed esters. On the other hand, vinyl acetate and its by-products are more volatile, causing less chromatographic interference. Considering all the above-mentioned facts, we decide to employ vinyl acetate for the rest of the EKR studies.

The influence of solvent on the rate and selectivity of enzymatic reactions still lacks a rational explanation. However, there is a clear empirical evidence that the nature of the organic solvent wields strong influence on the stability and catalytic performance of the hydrolytic enzymes [92]. The polarity or hydrophobicity of the solvents play a key role in the solvent effects [93]. Since the solvation of the enzyme–substrate complex significantly differs in different solvents leading to changes in the conformational rigidity of the enzymes [94–96], penetration and occupation of the enzyme active site [97,98] as well as alteration of the solvation of the transition state [99–101], then it is obvious that the enzyme catalytic behavior can change drastically as well. It has been also shown that varying the solvent composition in binary mixtures of solvents had a profound impact on the enantiomeric ratio due to change in the equilibrium constant K_{eq} for thermodynamically distinct physical states [102]. Interestingly, in rare cases, an organic solvent can even alter the stereopreferance of the enzyme [103].

Application of so-called 'solvent strategy' or 'medium engineering' often assists an increase in the activity and selectivity of the lipase-catalyzed reactions. Therefore, in this study, various organic solvents with different log *P* values were selected to investigate the effect of the reaction medium on the substrate conversion, optical purity of EKR products and the *E*-values (Table 4), respectively. In this context, we attempted (Chirazyme L-2, C-3)-catalyzed transesterification experiments by screening polar (i.e. 1,4-dioxane, CH_3CN, acetone, EtOAc), semi-polar [i.e. THF, vinyl acetate (VA), CH_2Cl_2, 2-methyl-2-butanol (*tert*-amyl alcohol), $CHCl_3$], and relatively hydrophobic (i.e. $PhCH_3$) organic solvents, within which *rac*-**2** formed a homogenous solution. Probably the most frequently used organic solvents for lipase-catalyzed reactions, such as *tert*-butyl methyl ketone (TBME) and diisopropyl ether (DIPE), were omitted from these studies due to poor solubility of the substrate *rac*-**2**. The results shown in Table 4 indicated that the best catalytic efficiency of Chirazyme L-2, C-3 was observed when ethyl acetate (EtOAc), *tert*-amyl alcohol and $PhCH_3$ were used as the respective reaction media. Only these solvents favor ultra-selective transformation of *rac*-**2** (*E*>200) yielding enantiomerically enriched (*S*)-(+)-**2** and (*R*)-(+)-**3a** in a 99–99.9 % ee range with 50 % conv. (Table 4, entries 4, 8 and 10). These results are somewhat surprising, because all the three mentioned solvents are characterized rather by different log*P* values (0.29–2.52) suggesting that the polarity was not a decisive factor in this case. On the other hand, although EtOAc may act also as a reversible acetyl donor the enantioselectivity was not affected. Following the recommendations given by various solvent sustainability guides assessing environmental-risk of using organic solvents [104–111], it was clear that EtOAc is the best candidate for a reaction medium.

Another parameter that should have been taken into account is the reaction temperature. It is known that the enzyme activity and enantioselectivity are dependent on the reaction temperature. Simple elevation of the temperature by 10 °C can significantly boost the rate of lipase-catalyzed reactions; however, deterioration in enzyme enantioselectivity may also occur. Since the thermal stability of biocatalysts is one of the most important criteria for industrial applications, the effect of temperature on EKR of *rac*-**2** was also studied. Using the aforementioned optimal conditions found for the resolution of *rac*-**2**, the enantioselective transesterification in the presence of Chirazyme L-2, C-3 suspended in a mixture of vinyl acetate and EtOAc was investigated at 40, 50 and 60 °C (Table 5), respectively. The EKR reactions were terminated deliberately after 3 h. The conversion increased from 40 % to 49 % with an increase of temperature from 40 °C to 50 °C, and from 40 % to 50 % when the reaction was carried out at 60 °C. To our delight, the enantioselectivity has not only not deteriorated with the increase in the temperature, but it also improved significantly. As a matter of fact, the observation that the lipase selectivity increases at higher temperatures is very rare. Regrettably, we are unable to give an explanation for this phenomenon; however, Hult and co-workers [112] suggested that the unusual behavior of an increasing enantioselectivity with temperature can be explained by a strong entropy contribution on the free enthalpy difference between the transitions states of both enantiomers of the resolved racemate. Yet, since enzyme activity was found to be the highest at 60 °C, while maintaining excellent enantioselectivity (*E*>200), 60 °C was selected as the optimal temperature for this reaction.

To demonstrate the usefulness of the enzymatic protocol 250 mg and 1 g of the substrate *rac*-**2** was used for each EKR (Table 6). Of course, the up-scaling procedure assumed the linear (proportional) enlargement of all the previously set parameters including the amounts of lipase and vinyl acetate as well as the solvent volume to remain reagents/catalysts at the same concentrations as previously. Since two parameters of EKR of *rac*-**2** were changed after preliminary kinetics analyses, a series of additional time-course experiments were conducted to gain insights into the reactions carried out at preparative scales in EtOAc at 60 °C. It is important to mention that in the present optimization study, HPLC analyses were performed simultaneously in one run using aliquots withdrawn directly from the crude reaction mixtures after the stipulated period of time (1–4 h) and in a one-hour intervals. This was done arbitrarily in order to save the consumption of both the lipase and substrate *rac*-**2**. The performed experiments revealed that excellent *E*-values can be reached regardless of the reaction scale, and what is even more spectacular, that in both cases the results provided evidence of the high repeatability of the developed process. It turned out that the optimal time after which the reactions should be terminated/arrested in order to obtain *E*>200 and 50 % conv. is about 2 h. More importantly, the astonishing enantiomeric resolution of the racemate *rac*-**2** resulting in pure enantiomers (*S*)-(+)-**2** and (*R*)-(+)-**3a** was observed in a 1g-scale EKR attempt (Table 6, entry 6).

In order to further evaluate the feasibility of the optimized EKR process for the synthesis of both enantiomers of lisofylline (**2**), the preparative-scale reactions were conducted again followed this time by a chromatographic purification step to establish the isolated yield of the optically active products (Table 7). Surprisingly, this time the EKRs of *rac*-**2** revealed some inconsistencies with the previously obtained results showing that the kinetic control had to be performed with greater

accuracy and caution especially when the reaction rates are relatively high as for a routine enantiomers resolution bioprocess. As a matter of fact, this showed that it might be reasonable to slightly elongate the reaction time by decreasing enzyme loading and/or lowering temperature. Nevertheless, EKR products (*S*)-(+)-**2** and (*R*)-(+)-**3a** were isolated in high 46–50 % yields with $E>200$ at 47–51 % conv., respectively.

In order to enlighten the capacity of lipase B from *Candida antarctica* to catalyze enantioselective lisofylline (*rac*-**2**) acetylation, molecular docking simulations were performed using freely available for noncommercial use open-source AutoDock Vina vs. 1.1.2 software [43]. For docking calculations, the X-ray crystal structure of CAL-B (PDB code: 1TCA) [45] was utilized as the receptor molecule. However, since the mechanism of lipase-catalyzed transesterification of alcohols involves the preceding acetylation of the catalytic serine by the acetyl donor (vinyl acetate in this case) [113], the side chain hydroxyl of the Ser105 of CAL-B was replaced by an acetate to mimic the formation of the acetyl-lipase intermediate. Only then, the resulting acetyl-lipase structure was taken as a target for the docking of both enantiomers of lisofylline substrate [(*R*)-(–)-**2** and (*S*)-(+)-**2**]. The energetically favorable poses in terms of binding energies [expressed as ΔG (kcal/mol)] of the substrates (*R*)-(–)-**2** and (*S*)-(+)-**2** binding to the active site of the acetyl-CAL-B were extracted and optimized from the results obtained by using the hybrid Lamarckian Genetic Algorithm (GA). After detail docking conformational search and examination of all the productive and unproductive binding poses for both the CAL-B-enantiomers' complexes it was clear which stereoisomer was able to form stable conformations compatible with the attack of the activated nucleophilic hydroxyl group of the substrate molecule **2** at the electrophilic carbon atom of the acetyl group of the catalytic serine-bound acetate. The preferred binding poses for both enantiomers are shown in Fig. 3. It is worth to note that near attack conformations (NACs) are conformers in which the atoms involved in the bond formation are at van der Waals distance (up to 4.0 Å) and the angle of approach is ±15° of the angle of the bond formed in the transition state (TS) [114–117]. Moreover, NACs are turnstiles through which the reactants must pass to reach the appropriate TS desired for successful catalysis. A higher population of the NACs indicates a lower free energy change required to reach the TS, thus the population of NACs is indicative of the reaction rate and the reactivities of conformations of both lisofylline enantiomers (*R*)-(–)-**2** and (*S*)-(+)-**2** in this case. Concerning CAL-B-catalyzed biotransformation of lisofylline (*rac*-**2**), the OH group of the favored substrate (*R*)-(–)-**2** is located close to the catalytic triad, with distances of 4.1 Å to electrophilic carbon atom of Ser105-acetyl. In this binding mode, all the hydrogen bonds required for catalysis including the normal stabilization of the oxyanion can occur as (*R*)-(–)-**2** is additionally stabilized by strong H-bond of 2.1 Å distance formed between hydrogen atom of the hydroxyl moiety of the ligand and the oxygen atom of the OH group of Thr40 residue, respectively. More specifically, hydrophobic CH—CH interactions between terminal methyl group of acetate moiety present in Ser105-acetyl residue and the methyl group directly bounded to a chiral stereogenic center of (*R*)-(–)-**2** were observed. Moreover, to avoid steric clashes the bulky substituent (3,9-dimethylxanthine ring) of the favored enantiomer (*R*)-(–)-**2** is readily accommodated in the larger hydrophobic cavity surrounded by the subsequent aliphatic amino acids: Ile285, Gln157, Leu140, and Ala141. In sharp contrast, the slow-reacting enantiomer (*S*)-(+)-**2** cannot undergo any favorable stabilization of the oxyanion tetrahedral intermediate due to steric reasons, suggesting that acylation on its OH group cannot occur. In addition, optimized binding mode of (*S*)-(+)-**2** in CAL-B catalytic cavity revealed that the alkyl side chain with the hydroxyl moiety is pulled far away from both the catalytic triad and the oxyanion hole. In this case, unproductive conformation of (*S*)-(+)-**2** is additionally persisted by strong 2.7 Å-long hydrogen bond interaction involving ligand's hydroxyl group and the oxygen atom of the carboxylic moiety of Leu140 residue located at the cavity bottom. In this case, CH—CH interactions between both methyl groups of acetate moiety in Ser105-acetyl residue and the one substituting N-3 atom of xanthine ring were also found. In conclusion, as the stereochemical architecture of the CAL-B catalytic pocket forces the

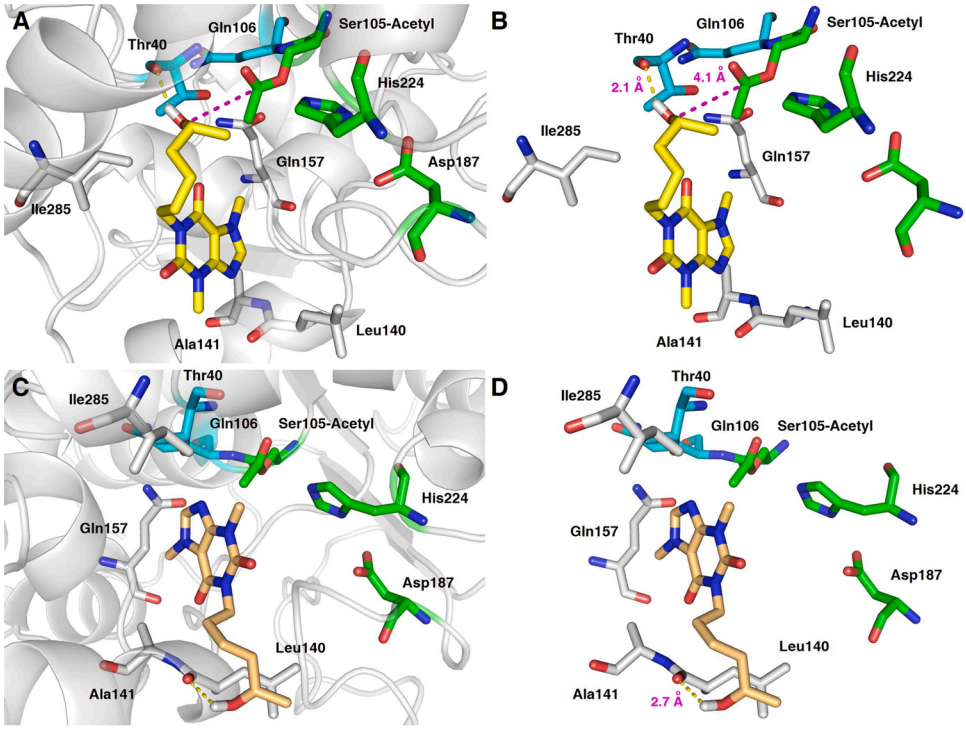

Fig. 3. Three-dimensional model of predominant conformations of (*R*)-(–)-**2** (yellow sticks) (see **A**–**B**) and (*S*)-(+)-**2** (light-orange sticks) (see **C**–**D**) in the active site of CAL-B (PDB code: 1TCA; shown as a gray-colored cartoon diagram with transparency set at 50 %). The residues constituting the catalytic triad (Ser105-acetyl-His224-Asp187) of CAL-B are shown in green sticks representation. The oxyanionic Thr40 and Gln106 residues are shown in cyan. The rest of the most significant residues contributing to the stabilization of *rac*-**2** enantiomers by polar interactions (yellow dashed lines) and by CH—CH van der Waals (vdW) interactions are shown in gray sticks representation. Nitrogen atoms are presented with blue colour, whereas the oxygen atoms with red colour. The selected mutual distances between the respective amino acid residues, and the ligands' atoms are given in Ångström. The different orientation of the enantiomers (*R*)-(–)-**2** and (*S*)-(+)-**2** toward acetyl-Ser105 and Thr40/Gln106 residues is clearly visible. In optimized poses of both substrates only the faster-reacting (*R*)-enantiomer (see **A**–**B**) is near the carbonyl oxygen atom of the serine bound acetate (acetyl-Ser105, 4.1 Å; the distances are indicated by magenta dashed lines) and additionally stabilized through the formation of hydrogen bond (yellow dashes) with the Thr40 residue (2.1 Å) (For interpretation of the references to colour in this figure legend, the reader is referred to the web version of this article.).

enantiomers of lisofylline (*rac*-**2**) to accommodate in two alternate orientations within both the catalytic triad and the oxyanion hole residues, thus a remarkable difference in the reaction rates of the enzymatic transformation of *rac*-**2** might be rationalized.

Following the observed results in our previous work for the CAL-B-catalyzed resolutions of racemic proxyphyline esters [78], we assumed that lisofylline acetate *rac*-**3a** could also constitute a perfect substrate for lipases, and what is even more optimistic, that the performed hydrolytic approach toward *rac*-**3a** might allow furnishing desired (*R*)-lisofylline [(*R*)-(–)-**2**] directly, without need for additional base-mediated deacetylation of the respective ester. Since solubility of acetate *rac*-**3a** in water turned out to be highly limited as well as considering the common fact that enzyme hydrolytic processes performed in aqueous solutions are rather harmful for scalability and potential industrialization (due to relatively low concentration of substrates/products, tedious product isolation and purification procedures including liquid-liquid extraction work up with frequently accompanying stable emulsions etc.), we decided to employ methanolytic approach using homophasic CH_3CN/MeOH mixture as the reaction system. The results of preliminary investigations are presented in Table 8.

However, our high expectations for the lipase-catalyzed methanolysis of *rac*-**3a** were disappointed when lower reaction rates as well deteriorated enantioselectivities were found in terms of the observed *E*-values when compared to transesterification approach. In consequence, enantiomeric purities of the slower-reacting enantiomer (*S*)-(–)-**3a** were obviously far from optimal (38–72 % ee). It is worth to note that enzyme screening for enantioselective methanolysis of *rac*-**3a** revealed that only CAL-B preparations proved to be potent to catalyze the reactions; however, with only 28–42 % conv. achievable within a 48-h time span. Other tested enzymes remained inactive toward *rac*-**3a** or catalyzed methanolytic EKR with residual substrate conversions. Nevertheless, this protocol might be considered as stereo-complementary toward lipase-catalyzed (trans)esterification since it allowed to obtain homochiral (*R*)-(–)-**2** (>99 % ee).

3.3. Approaches to the Preparation of (R)-Lisofylline [(R)-(–)-2]

In order to obtain pharmacologically active (*R*)-lisofylline [(*R*)-(–)-**2**], our next goal was to find optimal reaction conditions for hydrolysis of optically pure acetate (*R*)-(+)-**3a** (Table 9). Although deacetylation of (*R*)-(+)-**3a** with aqueous HCl had already been reported [22], we found this method defective as it yielded a partially racemized (*R*)-(–)-**2**. Therefore, acidic conditions were replaced by relatively mild basic conditions employing anhydrous potassium carbonate suspended in methanol. The K_2CO_3-mediated methanolysis strategy toward (*R*)-(+)-**3a** showed that all three reaction parameters, including the amount of base, reaction time and temperature, were crucial for successful deprotection of the acetyl group from hydroxyl moiety without affecting enantiomeric purity of the product (*R*)-(–)-**2**. When 4 equiv of K_2CO_3 were applied in the reaction mixture stirred at 25 °C, total consumption of the starting material (*R*)-(+)-**3a** was achieved after 24 h; however, desired (*R*)-(–)-**2** was obtained with 70 % ee. In the next experiment, the amount of base was reduced by half leading to >99 % conv., and hardly any racemization was observed. To eliminate a drop in enantiomeric excess of (*R*)-(–)-**2** further reduction in base concentration as well as reaction temperature were executed. The optical purity of (*R*)-(–)-**2** still testified of a negligible racemization of the title API. In addition, only 84 % conv. was detected under the applied conditions. Fortunately, shortening the reaction time to 18 h at 22 °C and leaving K_2CO_3 at 2 equiv level in respect to substrate (*R*)-(+)-**3a** furnished (*R*)-(–)-**2** in total enantiopurity and conversion, while the isolated yield reached 59 %. Relatively low isolated yield when compared with quantitative conversion values is probably due to the loss of the product (*R*)-(–)-**2** during column chromatography.

In the project continuation we searched for optimal reaction conditions for the inversion of the absolute configuration of the remaining (*S*)-(+)-**2**. Despite the fact that optical inversion of (*S*)-(+)-**2** had already been reported using Mitsunobu esterification with benzoic acid, triphenylphosphine (Ph_3P) and diethyl azodicarboxylate (DEAD) in THF [29,30], in order to avoid troublesome separation of the formed triphenylphosphine oxide from the reaction product an alternative methodology was elaborated.

In the first step, the hydroxyl moiety in (*S*)-(+)-**2** was converted into a better leaving group, that is a methanesulfonate. The mesylation of (*S*)-(+)-**2** was accomplished with 1.5 equiv of mesyl chloride and 1.5 equiv of Et_3N as a base in dry CH_2Cl_2 at ambient temperature. After a 1-h reaction the optically pure mesylate (*S*)-(+)-**4** (>99 % ee) was isolated in 68 % yield. Next, the ability of stereoselective acetolysis of (*S*)-(+)-**4** was examined by using cesium acetate (CsOAc) as a nucleophile in the presence of catalytic amount of crown ether (18-crown-6) (Table 10). The screening of the reaction conditions for substitution of mesyl group *via* a direct S_N2-like displacement by acetate ion was initiated in dry $PhCH_3$ as a solvent. The optimal reaction conditions were obtained when mesyl derivative (*S*)-(+)-**4** was exposed to 2 equiv of CsOAc in dry $PhCH_3$ while heating the mixture at 110 °C for 18 h. The high selectivity achieved with this system allowed to obtain (*R*)-(+)-**3a** (96 % ee) in 50

Table 9
Optimization of the reaction conditions for the K_2CO_3-mediated methanolysis of (*R*)-(+)-**3a**.

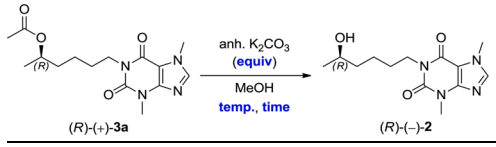

Entry	K_2CO_3 [equiv]	*t* [h]	*T* [°C]	Conv.[a] [%]/Yield[b] [%]	ee[c] [%]
1	4[d]	24	25	>99/N.D.[e]	70
2	2[d]	24	25	>99/N.D.[e]	98
3	1[d]	24	20	84/N.D.[e]	98
4	2[f]	18	22	>99/59	99

[a] Determined by GC.
[b] Isolated yield after column chromatography eluted with gradient of $CHCl_3$/MeOH (98:2, 95:5 v/v) mixture.
[c] Enantiomeric excess of (*R*)-(–)-**2** determined by chiral HPLC analysis using a Chiralpak AD-H column.
[d] Conditions: (*R*)-(+)-**3a** (20 mg, 62 μmol, 99 % ee), anhydrous K_2CO_3 (1–4 equiv.), MeOH (2 mL).
[e] Not determined.
[f] Conditions: (*R*)-(+)-**3a** (100 mg, 0.31 mmol, 99 % ee), anhydrous K_2CO_3 (2 equiv.), MeOH (10 mL).

Table 10
Optimization of the stereoinversion reaction conditions for the optically active mesylate (*S*)-(+)-**4**.

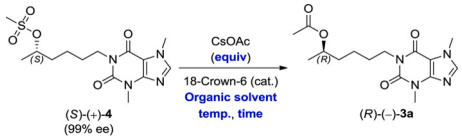

Entry	CsOAc [equiv][a]	Solvent	*t* [h]	*T* [°C]	Conv.[b] [%]/Yield[c] [%]	ee[d] [%]
1	2	$PhCH_3$	24	RT	<20/N.D.[e]	N.D.[e]
2	1	$PhCH_3$	48	110	>99/19	86
3	2	$PhCH_3$	18	110	>99/50	96
4	2	DMF	18	50	>99/40	95

[a] Conditions: (*S*)-(+)-**4** (10 mg, 27.9 μmol, 99 % ee), CsOAc (1–2 equiv.), 18-Crown-6 (cat.), dry solvent (2 mL).
[b] Determined by GC.
[c] Isolated yield after column chromatography eluted with pure EtOAc.
[d] Enantiomeric excess of (*R*)-(–)-**2** determined by chiral HPLC analysis using a Chiralpak AD-H column.
[e] Not determined.

% yield with only partial loss of optical purity (Δ% ee = 3) and without detecting of elimination by-product (Table 10, entry 3). In dry DMF, ester formation was facilitated even at 50 °C (>99 % conv.); however, transformation of (*S*)-(+)-**4** resulted in a slightly less selective manner and in a lower yield. The resulting acetate (*R*)-(+)-**3a** was then converted back to the free alcohol (*R*)-(–)-**2** *via* previously elaborated saponification of the ester with K_2CO_3 in methanol.

3.4. Determination of absolute configuration of lisofylline enantiomers (2)

The absolute configuration assignment of both lisofylline enantiomers (**2**) was done by simple comparison of the experimental results concerning the specific signs of optical rotation with literature data (see Supporting Information) as well as peaks' elution order of chiral high-performance liquid chromatography (*C*-HPLC) analyses (Fig. 4).

In addition to polarimetric and LC chromatographic correlative studies, the absolute configuration of non-racemic API **2** was undeniably established by solving X-ray crystal structures for the respective single crystals obtained for each enantiomer (*R*)-(–)-**2** (Fig. 5) and (*S*)-(+)-**2** (Fig. 6). The crystals with sufficient quality for single-crystal X-ray diffraction analyses were obtained using a conventional vapor diffusion crystallization technique (VDCT) employing EtOAc as the solvent and *n*-hexane as the precipitant (see paragraph 2.15.1. in Experimental section). To the best of our knowledge, the crystal structures of neither racemic nor enantiomeric lisofylline (**2**) obtained from single-crystal X-ray experiments have been reported until now. Therefore, these studies may pave the way for further analyses of i.e. the polymorphic behavior of racemic and enantiopure lisofylline (**2**), which is a crucial factor from the point of view of bioavailability, biological activity and safety of medication. The ORTEP drawings of both lisofylline enantiomers (*R*)-(–)-**2** and (*S*)-(+)-**2** were prepared using freeware crystallographic software (ORTEP-3 for Windows) developed by Louis J. Farrugia [118].

4. Conclusions

The present study reports on the first example of concise, highly enantioselective, and stereoconvergent chemoenzymatic syntheses of lisofylline enantiomers achieved in 3 and 5 reaction steps, respectively. The key transformation was classical enzymatic kinetic resolution of racemic lisofylline. For this purpose, a set of commercially available lipase preparations were screened and extensively manipulated in a

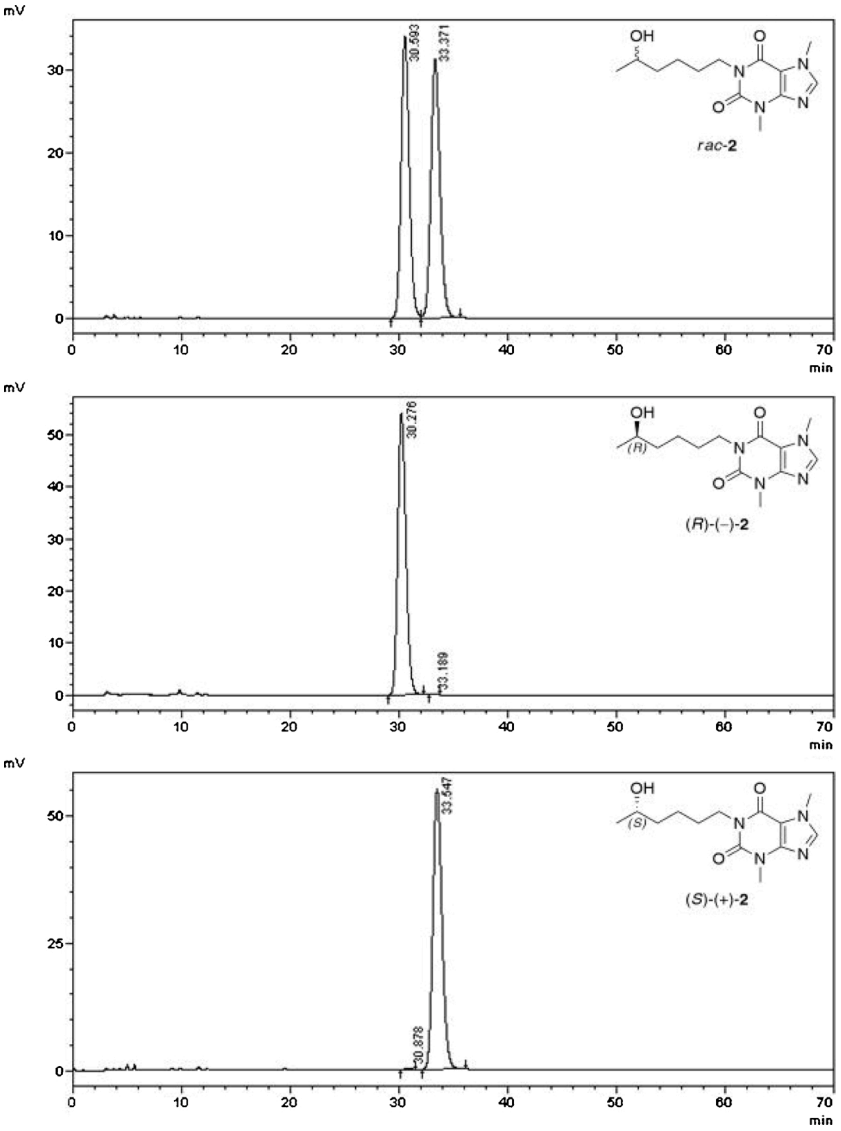

Fig. 4. HPLC chiral analyses of racemic lisofylline (*rac*-**2**), and its single enantiomers (*R*)-(–)-**2** and (*S*)-(+)-**2**. Chromatographic conditions are shown in Supporting Information.

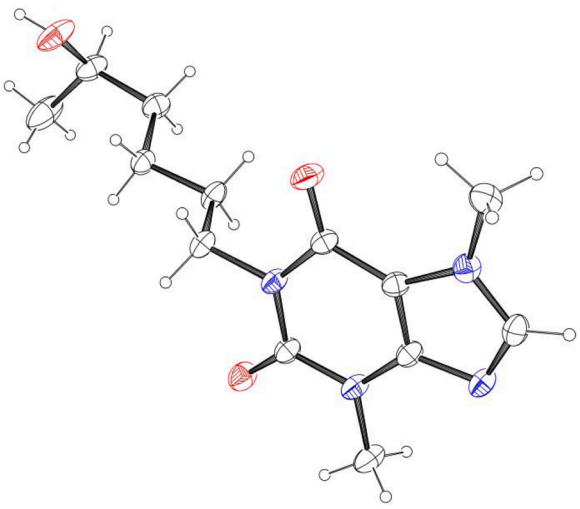

Fig. 5. An ORTEP plot of (*R*)-lisofylline [(*R*)-(–)-**2**]. Thermal ellipsoids were drawn at 50 % probability (C black, H gray, N blue, O red). The following crystal structure was deposited at the Cambridge Crystallographic Data Centre and allocated the deposition number CCDC-2023424 (For interpretation of the references to colour in this figure legend, the reader is referred to the web version of this article.).

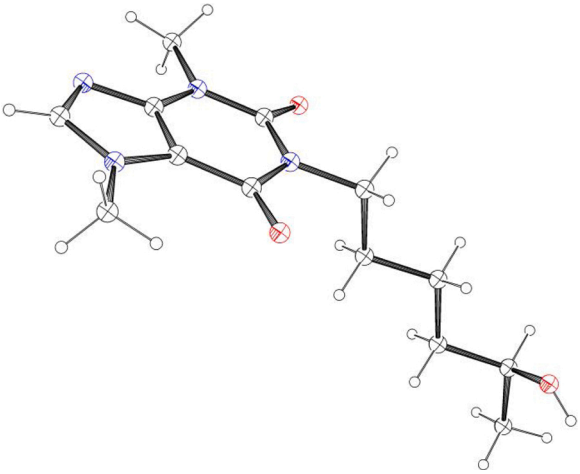

Fig. 6. An ORTEP plot of (*S*)-lisofylline [(*S*)-(+)-**2**]. Thermal ellipsoids were drawn at 50 % probability (C black, H gray, N blue, O red). The following crystal structure was deposited at the Cambridge Crystallographic Data Centre and allocated the deposition number CCDC-2023425 (For interpretation of the references to colour in this figure legend, the reader is referred to the web version of this article.).

transesterification mode using different acyl donors and organic solvents as well as various reaction temperatures. The most enantioselective lipase-catalyzed KR protocol, yielding both resolution products in homochiral form (>99 % ee), was accomplished with the biocatalytic system composed of commercial Chirazyme L-2, C-3 preparation and 3 equiv of vinyl acetate in EtOAc at 60 °C. In further experiments, an enzymatic ultra-selective stereochemical discrimination of lisofylline enantiomers was successfully scaled up to a 1-gram of racemic substrate thus affording both optically pure EKR products in 47–50 % yield range, respectively. Further chemical functionalization of the slower-reacting (*S*)-(+)-enantiomer of lisofylline (>99 % ee) into the respective (*S*)-(+)-mesylate (99 % ee) followed by nucleophilic substitution using 2 equiv of CsOAc in the presence of 18-Crown-6 in boiling $PhCH_3$ and the subsequent K_2CO_3-mediated methanolysis of the formed (*R*)-acetate (98 % ee) resulted in the formation of (*R*)-(–)-lisofylline (96 % ee) isolated in 20 % overall yield after 3 steps. The total yield of enantioenriched (*R*)-configurated lisofylline using this convergent route was 28.8 %, including 8.9 % overall yield for synthesis consisting of linear sequence of 5 steps and 19.9 % overall yield for 3 reaction steps synthesis, and thus seems to be slightly improved when compared with the procedure reported by Drosos et al. [27] (21.8 % overall yield after 4 steps) making it a promising and competitive for practical application. Moreover, XRD crystal structures of both enantiomers of titled lisofylline have never been accessed before and will be of great importance with respect to future investigation into this pharmaceutical. In addition, in order to better understand the observed stereochemical outcome of CAL-B-catalyzed enantioselective transesterification of *rac*-**2**, we generated a binding mode proposal for the lowest binding potential energy complexes of the Ser105-acetylated CAL-B active-site with (*R*)-(–)-**2** and (*S*)-(+)-**2**, respectively, based on X-ray crystal structure of the employed lipase and computational docking simulations. The close distance between the catalytic acetylated-serine in the active site and the hydroxyl function of the ligand molecule as well as necessary H-bonding stabilizing the formation of oxyanion for effective catalysis occur only in the complex of CAL-B and (*R*)-(–)-**2**. In contrary, oxyanion-stabilizing H-bonds in the non-productive complex of CAL-B and (*S*)-(+)-**2** are lost, and the distance between catalytically active acylated serine and the hydroxyl function is too long to obtain the formation of the second tetrahedral intermediate and overall effective catalysis.

CRediT authorship contribution statement

Paweł Borowiecki: Conceptualization, Methodology, Validation, Investigation, Data curation, Writing - original draft, Writing - review & editing, Funding acquisition, Supervision, Software, Project administration. **Beata Zdun:** Investigation. **Maciej Dranka:** Investigation.

Declaration of Competing Interest

The authors report no declarations of interest.

Acknowledgements

This research was financially supported by the National Science Centre (NCN) of Poland in the framework of grant SONATA 15 (No: 2019/35/D/ST4/01556). The Warsaw University of Technology, Faculty of Chemistry is appreciated (statute work). B.Z. acknowledges financial support from IDUB project ('Scholarship Plus' programme).

Appendix A. Supplementary data

Supplementary material related to this article can be found, in the online version, at doi:https://doi.org/10.1016/j.mcat.2021.111451.

References

[1] Methylxanthines, in: B.B. Fredholm (Ed.), Handbook of Experimental Pharmacology, Vol. 200, Springer-Verlag, Berlin Heidelberg, 2011.
[2] M. Walczak, J. Szymura-Oleksiak, E. Pekala, Validation of a high-performance liquid chromatography method for pharmacokinetic evaluation of pentoxifylline and lisofylline in rat serum and tissues, Acta Pol. Pharm. 66 (3) (2009) 215–224. http://www.ncbi.nlm.nih.gov/pubmed/19645320.
[3] J.A. Lillibridge, T.F. Kalhorn, J.T. Slattery, Metabolism of lisofylline and pentoxifylline in human liver microsomes and cytosol, Drug Metab. Dispos. 24 (11) (1996) 1174–1179. https://dmd.aspetjournals.org/content/24/11/1174.
[4] J.J. Bright, C. Du, M. Coon, S. Sriram, S.J. Klaus, Prevention of experimental allergic encephalomyelitis via inhibition of IL-12 signaling and IL-12-mediated Th1 differentiation: an effect of the novel anti-inflammatory drug lisofylline, J. Immunol. 161 (12) (1998) 7015–7022. http://www.jimmunol.org/content/161/12/7015.
[5] M.E. Coon, M. Diegel, N. Leshinsky, S.J. Klaus, Selective pharmacologic inhibition of murine and human IL-12-dependent Th1 differentiation and IL-12 signaling, J. Immunol. 163 (12) (1999) 6567–6574. http://www.jimmunol.org/content/163/12/6567.

[6] A. Jankowska, A. Swierczek, G. Chlon-Rzepa, M. Pawlowski, E. Wyska, PDE7-Selective and dual inhibitors: advances in chemical and biological research, Curr. Med. Chem. 24 (7) (2017) 673–700, https://doi.org/10.2174/0929867324666170116125159.

[7] A. Swierczek, E. Wyska, S. Bas, M. Woyciechowska, J. Mlynarski, PK/PD studies on non-selective PDE inhibitors in rats using cAMP as a marker of pharmacological response, Naunyn Schmiedebergs Arch. Pharmacol. 390 (10) (2017) 1047–1059, https://doi.org/10.1007/s00210-017-1406-z.

[8] Z. Yang, M. Chen, L.B. Fialkow, J.D. Ellett, R. Wu, J.L. Nadler, Inhibition of STAT4 activation by lisofylline is associated with the protection of autoimmune diabetes, Ann. N. Y. Acad. Sci. 1005 (2003) 409–411, https://doi.org/10.1196/annals.1288.069.

[9] G.C. Rice, J. Rosen, R. Weeks, J. Michnick, S. Bursten, J.A. Bianco, J.W. Singer, CT-1501R selectively inhibits induced inflammatory monokines in human whole blood ex vivo, Shock 1 (4) (1994) 254–266, https://doi.org/10.1097/00024382-199404000-00003.

[10] G.C. Rice, P.A. Brown, R.J. Nelson, J.A. Bianco, J.W. Singer, S. Bursten, Protection from endotoxic shock in mice by pharmacologic inhibition of phosphatidic acid, Proc. Natl. Acad. Sci. U. S. A. 91 (9) (1994) 3857–3861, https://doi.org/10.1073/pnas.91.9.3857.

[11] S. Wattanasirichaigoon, M.J. Menconi, M.P. Fink, Lisofylline ameliorates intestinal and hepatic injury induced by hemorrhage and resuscitation in rats, Crit. Care Med. 28 (5) (2000) 1540–1549, https://doi.org/10.1097/00003246-200005000-00047.

[12] A. Swierczek, E. Wyska, K. Pociecha, S. Bas, J. Mlynarski, Influence of inflammatory disorders on pharmacokinetics of lisofylline in rats: implications for studies in humans, Xenobiotica 49 (10) (2019) 1209–1220, https://doi.org/10.1080/00498254.2018.1542516.

[13] S.L. Bursten, D. Federighi, J. Wald, B. Meengs, W. Spickler, E. Nudelman, Lisofylline causes rapid and prolonged suppression of serum levels of free fatty acids, J. Pharmacol. Exp. Ther. 284 (1) (1998) 337–345. https://jpet.aspetjournals.org/content/284/1/337.

[14] P. de Vries, J.W. Singer, Lisofylline suppresses ex vivo release by murine spleen cells of hematopoietic inhibitors induced by cancer chemotherapeutic agents, Exp. Hemat. 28 (8) (2000) 916–923, https://doi.org/10.1016/s0301-472x(00)00493-8.

[15] T.C. Peterson, M.R. Peterson, J.M. Raoul, The effect of pentoxifylline and its metabolite-1 on inflammation and fibrosis in the TNBS model of colitis, Eur. J. Pharmacol. 662 (1-3) (2011) 47–54, https://doi.org/10.1016/j.ejphar.2011.04.030.

[16] M. Chen, Z. Yang, R. Wu, J.L. Nadler, Lisofylline, a novel antiinflammatory agent, protects pancreatic beta-cells from proinflammatory cytokine damage by promoting mitochondrial metabolism, Endocrinology 143 (6) (2002) 2341–2348, https://doi.org/10.1210/endo.143.6.8841.

[17] Z.D. Yang, M. Chen, R. Wu, M. McDuffie, J.L. Nadler, The anti-inflammatory compound lisofylline prevents Type I diabetes in non-obese diabetic mice, Diabetologia 45 (9) (2002) 1307–1314, https://doi.org/10.1007/s00125-002-0901-y.

[18] J.S. Striffler, J.L. Nadler, Lisofylline, a novel anti-inflammatory agent, enhances glucose-stimulated insulin secretion in vivo and in vitro: studies in prediabetic and normal rats, Metabolism 53 (3) (2004) 290–296, https://doi.org/10.1016/j.metabol.2003.10.008.

[19] D. Bleich, Lisofylline, an inhibitor of unsaturated phosphatidic acid generation, ameliorates interleukin-1 beta-induced dysfunction in cultured rat islets, Endocrinology 137 (11) (1996) 4871–4877, https://doi.org/10.1210/endo.137.11.8895359.

[20] M. Nicklasson, S. Bjorkman, B. Roth, M. Jonsson, P. Hoglund, Stereoselective metabolism of pentoxifylline in vitro and in vivo in humans, Chirality 14 (8) (2002) 643–652, https://doi.org/10.1002/chir.10121.

[21] J.M. Raoul, M.R. Peterson, T.C. Peterson, A novel drug interaction between the quinolone antibiotic ciprofloxacin and a chiral metabolite of pentoxifylline, Biochem. Pharmacol. 74 (4) (2007) 639–646, https://doi.org/10.1016/j.bcp.2007.05.013.

[22] J.P. Klein, A.M. Kumar, A.J. Leigh, J. Michnick, G.E. Underiner, Asymmetric synthesis of chiral secondary alcohols, Patent WO9531450A1, 1995.

[23] P. Cui, T.L. Macdonald, M. Chen, J.L. Nadler, Synthesis and biological evaluation of lisofylline (LSF) analogs as a potential treatment for Type 1 diabetes, Bioorg. Med. Chem. Lett. 16 (13) (2006) 3401–3405, https://doi.org/10.1016/j.bmcl.2006.04.036.

[24] J. Bianco, D. Porubek, J. Singer, P. Woodson, R-enatiomerically pure hydroxylated xanthine compounds to treat baldness, Patent US5567704A, 1996.

[25] X.H. Yang, K. Wang, S.F. Zhu, J.H. Xie, Q.L. Zhou, Remote ester group leads to efficient kinetic resolution of racemic aliphatic alcohols via asymmetric hydrogenation, J. Am. Chem. Soc. 136 (50) (2014) 17426–17429, https://doi.org/10.1021/ja510990v.

[26] L. Wang, J. Xie, X. Yang, Q. Zhou, Kinetic resolution of racemic hydroxy ester via asymmetric catalytic hydrogenation and application thereof, Patent US2017334831A1, 2017.

[27] N. Drosos, B. Morandi, Boron-catalyzed regioselective deoxygenation of terminal 1,2-Diols to 2-Alkanols enabled by the strategic formation of a cyclic siloxane intermediate, Angew. Chem. Int. Ed. Engl. 54 (30) (2015) 8814–8818, https://doi.org/10.1002/anie.201503172.

[28] P.J. Davis, S.K. Yang, R.V. Smith, Microbial models of mammalian metabolism: microbial reduction and oxidation of pentoxifylline, Appl. Environ. Microbiol. 48 (2) (1984) 327–331, https://doi.org/10.1128/AEM.48.2.327-331.1984.

[29] W. Aretz, H. Furrer, U. Gebert, H.-J. Hinze, Verfahren zur enantioselektiven darstellung von ((omega)-1)-hydroxyalkylxanthinen, Patent DE3942872A1, 1991.

[30] W. Aretz, H. Furrer, U. Gebert, H.-J. Hinze, 7-methoxymethly-3-methyl-1-(5-oxohexyl)xanthine, Patent US5710272A, 1998.

[31] E. Pekala, A. Godawska-Matysik, D. Zelaszczyk, Enantioselective reduction of pentoxifylline to lisofylline using whole-cell Lactobacillus kefiri biotransformation, Biotechnol. J. 2 (4) (2007) 492–496, https://doi.org/10.1002/biot.200600236.

[32] K. Wojcik-Pszczola, K. Hincza, D. Wnuk, D. Kadziolka, P. Koczurkiewicz, M. Sanak, Z. Madeja, E. Pekala, M. Michalik, Pentoxifylline and its active metabolite lisofylline attenuate transforming growth factor beta1-induced asthmatic bronchial fibroblast-to-myofibroblast transition, Acta Biochim. Pol. 63 (3) (2016) 437–442, https://doi.org/10.18388/abp.2016_1357.

[33] E. Pękala, T. Wójcik, Enantioselective biotransformation of pentoxifylline into lisofylline using wine yeast biocatalysis, Acta Pol. Pharm. 64 (2007) 109–113. https://www.ptfarm.pl/pub/File/Acta_Poloniae/2007/2/109.pdf.

[34] E. Pękala, Alcohol dehydrogenases as tools for the preparation of enantiopure metabolites of drugs with methyl alkyl ketone moiety, Sci. Pharm. 77 (1) (2009) 9–17, https://doi.org/10.3797/scipharm.0901-26.

[35] A.T. Larsen, E.M. May, K. Auclair, Predictable stereoselective and chemoselective hydroxylations and epoxidations with P450 3A4, J. Am. Chem. Soc. 133 (20) (2011) 7853–7858, https://doi.org/10.1021/ja200551y.

[36] P. Schiavini, K.J. Cheong, N. Moitessier, K. Auclair, Active site crowding of cytochrome P450 3A4 as a strategy to alter its selectivity, ChemBioChem 18 (3) (2017) 248–252, https://doi.org/10.1002/cbic.201600546.

[37] O.V. Dolomanov, L.J. Bourhis, R.J. Gildea, J.A.K. Howard, H. Puschmann, OLEX2: a complete structure solution, refinement and analysis program, J. Appl. Crystallogr. 42 (2) (2009) 339–341, https://doi.org/10.1107/S0021889808042726.

[38] G.M. Sheldrick, A short history ofSHELX, Acta Crystallogr., A, Found. Crystallogr. 64 (1) (2007) 112–122, https://doi.org/10.1107/S0108767307043930.

[39] G.M. Sheldrick, Crystal structure refinement withSHELXL, Acta Crystall. Sect. C Struct. Chem. 71 (1) (2015) 3–8, https://doi.org/10.1107/S2053229614024218.

[40] S. Parsons, H.D. Flack, T. Wagner, Use of intensity quotients and differences in absolute structure refinement, Acta Crystall. Sect. B Struct. Sci. Crystal Eng. Mat. 69 (3) (2013) 249–259, https://doi.org/10.1107/S2052519213010014.

[41] A.L. Spek, Structure validation in chemical crystallography, Acta Crystall. Sect. D Biol. Crystall. 65 (2) (2009) 148–155, https://doi.org/10.1107/S090744490804362X.

[42] R.W.W. Hooft, L.H. Straver, A.L. Spek, Determination of absolute structure using Bayesian statistics on Bijvoet differences, J. Appl. Crystall. 41 (1) (2008) 96–103, https://doi.org/10.1107/S0021889807059870.

[43] O. Trott, A.J. Olson, AutoDock Vina: improving the speed and accuracy of docking with a new scoring function, efficient optimization, and multithreading, J. Comput. Chem. 31 (2) (2010) 455–461, https://doi.org/10.1002/jcc.21334.

[44] E.F. Pettersen, T.D. Goddard, C.C. Huang, G.S. Couch, D.M. Greenblatt, E. C. Meng, T.E. Ferrin, UCSF Chimera–a visualization system for exploratory research and analysis, J. Comp. Chem. 25 (13) (2004) 1605–1612, https://doi.org/10.1002/jcc.20084.

[45] J. Uppenberg, M.T. Hansen, S. Patkar, T.A. Jones, The sequence, crystal structure determination and refinement of two crystal forms of lipase B from Candida antarctica, Structure 2 (4) (1994) 293–308, https://doi.org/10.1016/s0969-2126(00)00031-9.

[46] M.F. Sanner, Python: a programming language for software integration and development, J. Mol. Graph. Model. 17 (1) (1999) 57–61. http://www.ncbi.nlm.nih.gov/pubmed/10660911.

[47] A. Carvalho, T. Fonseca, M. Mattos, M. Oliveira, T. Lemos, F. Molinari, D. Romano, I. Serra, Recent advances in lipase-mediated preparation of pharmaceuticals and their intermediates, Int. J. Mol. Sci. 16 (12) (2015) 29682–29716, https://doi.org/10.3390/ijms161226191.

[48] D. Méndez-Sánchez, M. López-Iglesias, V. Gotor-Fernández, Hydrolases in organic chemistry. Recent achievements in the synthesis of pharmaceuticals, Curr. Org. Chem. 20 (11) (2016) 1186–1203. https://www.ingentaconnect.com/content/ben/coc/2016/00000020/00000011/art00005.

[49] D. Albarrán-Velo, V. González-Martínez, Gotor-Fernández, Stereoselective biocatalysis: a mature technology for the asymmetric synthesis of pharmaceutical building blocks, Biocatal. Biotransform. 36 (2) (2017) 102–130, https://doi.org/10.1080/10242422.2017.1340457.

[50] G. de María, A. de Gonzalo, Alcántara, Biocatalysis as useful tool in asymmetric synthesis: an assessment of recently granted patents (2014–2019), Catalysts 9 (10) (2019) 802, https://doi.org/10.3390/catal9100802.

[51] F.J. Contesini, M.G. Davanço, G.P. Borin, K.G. Vanegas, J.P.G. Cirino, R.Rd. Melo, U.H. Mortensen, K. Hildén, D.R. Campos, Pd.O. Carvalho, Advances in recombinant lipases: production, engineering, immobilization and application in the pharmaceutical industry, Catalysts 10 (9) (2020) 1032, https://doi.org/10.3390/catal10091032.

[52] K. Faber (Ed.), Biotransformations in Organic Chemistry: A Textbook, 7th ed., Springer Verlag, New York, NY, 2018.

[53] A. Salihu, M.Z. Alam, Solvent tolerant lipases: a review, Process. Biochem. 50 (1) (2015) 86–96, https://doi.org/10.1016/j.procbio.2014.10.019.

[54] P. Adlercreutz, Immobilisation and application of lipases in organic media, Chem. Soc. Rev. 42 (15) (2013) 6406–6436, https://doi.org/10.1039/c3cs35446f.

[55] M. Filice, J.M. Guisan, J.M. Palomo, Effect of ionic liquids as additives in the catalytic properties of different immobilized preparations of Rhizomucor miehei

lipase in the hydrolysis of peracetylated lactal, Green Chem. 12 (8) (2010) 1365–1369, https://doi.org/10.1039/c003829f.
[56] T. De Diego, A. Manjón, P. Lozano, M. Vaultier, J.L. Iborra, An efficient activity ionic liquid-enzyme system for biodiesel production, Green Chem. 13 (2) (2011) 444–451, https://doi.org/10.1039/c0gc00230e.
[57] J.V. Rodrigues, D. Ruivo, A. Rodríguez, F.J. Deive, J.M.S.S. Esperança, I. M. Marrucho, C.M. Gomes, L.P.N. Rebelo, Structural–functional evaluation of ionic liquid libraries for the design of co-solvents in lipase-catalysed reactions, Green Chem. 16 (10) (2014) 4520–4523, https://doi.org/10.1039/c4gc01329h.
[58] H.N. Hoang, T. Matsuda, Expanding substrate scope of lipase-catalyzed transesterification by the utilization of liquid carbon dioxide, Tetrahedron 72 (46) (2016) 7229–7234, https://doi.org/10.1016/j.tet.2015.11.052.
[59] S.H. Kim, S. Park, H. Yu, J.H. Kim, H.J. Kim, Y.-H. Yang, Y.H. Kim, K.J. Kim, E. Kan, S.H. Lee, Effect of deep eutectic solvent mixtures on lipase activity and stability, J. Mol. Catal., B Enzym. 128 (2016) 65–72, https://doi.org/10.1016/j.molcatb.2016.03.012.
[60] D. González-Martínez, V. Gotor, V. Gotor-Fernández, Application of deep eutectic solvents in promiscuous lipase-catalysed aldol reactions, Eur. J. Org. Chem. 2016 (8) (2016) 1513–1519, https://doi.org/10.1002/ejoc.201501553.
[61] Y. Zhang, X. Xia, M. Duan, Y. Han, J. Liu, M. Luo, C. Zhao, Y. Zu, Y. Fu, Green deep eutectic solvent assisted enzymatic preparation of biodiesel from yellow horn seed oil with microwave irradiation, J. Mol. Catal., B Enzym. 123 (2016) 35–40, https://doi.org/10.1016/j.molcatb.2015.10.013.
[62] N. Guajardo, P. Domínguez de María, K. Ahumada, R.A. Schrebler, R. Ramírez-Tagle, F.A. Crespo, C. Carlesi, Water as cosolvent: nonviscous deep eutectic solvents for efficient lipase-catalyzed esterifications, ChemCatChem 9 (8) (2017) 1393–1396, https://doi.org/10.1002/cctc.201601575.
[63] H.R. Hobbs, N.R. Thomas, Biocatalysis in supercritical fluids, in fluorous solvents, and under solvent-free conditions, Chem. Rev. 107 (6) (2007) 2786–2820, https://doi.org/10.1021/cr0683820.
[64] S.-H. Pyo, P. Persson, S. Lundmark, R. Hatti-Kaul, Solvent-free lipase-mediated synthesis of six-membered cyclic carbonates from trimethylolpropane and dialkyl carbonates, Green Chem. 13 (4) (2011) 976–982, https://doi.org/10.1039/c0gc00783h.
[65] N. El-Boulifi, S.E. Ashari, M. Serrano, J. Aracil, M. Martinez, Solvent-free lipase-catalyzed synthesis of a novel hydroxyl-fatty acid derivative of kojic acid, Enzyme Microb. Technol. 55 (2014) 128–132, https://doi.org/10.1016/j.enzmictec.2013.10.009.
[66] L. Corici, A. Pellis, V. Ferrario, C. Ebert, S. Cantone, L. Gardossi, Understanding potentials and restrictions of solvent-free enzymatic polycondensation of itaconic acid: an experimental and computational analysis, Adv. Synth. Catal. 357 (8) (2015) 1763–1774, https://doi.org/10.1002/adsc.201500182.
[67] J.G. Hernández, M. Frings, C. Bolm, Mechanochemical enzymatic kinetic resolution of secondary alcohols under ball-milling conditions, ChemCatChem 8 (10) (2016) 1769–1772, https://doi.org/10.1002/cctc.201600455.
[68] S. Kaabel, T. Friscic, K. Auclair, Mechanoenzymatic transformations in the absence of bulk water: a more natural way of using enzymes, ChemBioChem 21 (6) (2020) 742–758, https://doi.org/10.1002/cbic.201900567.
[69] S. Wu, R. Snajdrova, J.C. Moore, K. Baldenius, U. Bornscheuer, Biocatalysis: enzymatic synthesis for industrial applications, Angew. Chem. 59 (2020) 2–34, https://doi.org/10.1002/ange.202006648.
[70] Q. Wu, P. Soni, M.T. Reetz, Laboratory evolution of enantiocomplementary Candida antarctica lipase B mutants with broad substrate scope, J. Am. Chem. Soc. 135 (5) (2013) 1872–1881, https://doi.org/10.1021/ja310455t.
[71] Y. Wikmark, K. Engelmark Cassimjee, R. Lihammar, J.-E. Bäckvall, Removing the active-site flap in lipase a fromCandida antarcticaProduces a functional enzyme without interfacial activation, ChemBioChem: Eur. J. Chem. Biol. 17 (2) (2016) 141–145, https://doi.org/10.1002/cbic.201500471.
[72] Y. Cen, D. Li, J. Xu, Q. Wu, Q. Wu, X. Lin, Highly focused library-based engineering of candida antarctica lipase B with (S)-selectivity towards sec-alcohols, Adv. Synth. Catal. 361 (1) (2018) 126–134, https://doi.org/10.1002/adsc.201800711.
[73] Samah Hashim Albayati, Malihe Masomian, Siti Nor Hasmah Ishak, Mohd Shukuri bin Mohamad Ali, Adam Leow Thean, Fairolniza binti Mohd Shariff, Noor Dina binti Muhd Noor, Raja Noor Zaliha Raja Abd Rahman, Main structural targets for engineering lipase substrate specificity, Catalysts 10 (7) (2020) 747, https://doi.org/10.3390/catal10070747.
[74] P. Borowiecki, M. Dranka, A facile lipase-catalyzed KR approach toward enantiomerically enriched homopropargyl alcohols, Bioorg. Chem. 93 (2019) 102754, https://doi.org/10.1016/j.bioorg.2019.01.050.
[75] P. Borowiecki, N. Telatycka, M. Tataruch, A. Żądło-Dobrowolska, T. Reiter, K. Schühle, J. Heider, M. Szaleniec, W. Kroutil, Biocatalytic asymmetric reduction of γ-Keto esters to access optically active γ-aryl-γ-butyrolactones, Adv. Synth. Catal. 362 (10) (2020) 2012–2029, https://doi.org/10.1002/adsc.201901483.
[76] P. Borowiecki, D. Paprocki, M. Dranka, First chemoenzymatic stereodivergent synthesis of both enantiomers of promethazine and ethopropazine, Beilstein J. Org. Chem. 10 (2014) 3038–3055, https://doi.org/10.3762/bjoc.10.322.
[77] M. Poterała, M. Dranka, P. Borowiecki, Chemoenzymatic preparation of enantiomerically enriched (R)-(-)-Mandelic acid derivatives: application in the synthesis of the active agent pemoline, Eur. J. Org. Chem. 2017 (16) (2017) 2290–2304, https://doi.org/10.1002/ejoc.201700161.
[78] P. Borowiecki, D. Paprocki, A. Dudzik, J. Plenkiewicz, Chemoenzymatic synthesis of proxyphylline enantiomers, J. Org. Chem. 81 (2) (2016) 380–395, https://doi.org/10.1021/acs.joc.5b01840.
[79] P. Borowiecki, M. Młynek, M. Dranka, Chemoenzymatic synthesis of enantiomerically enriched diprophylline and xanthinol nicotinate, Bioorg. Chem. (2020) 104448, https://doi.org/10.1016/j.bioorg.2020.104448.
[80] U. Hanefeld, Reagents for (ir)reversible enzymatic acylations, Org. Biomol. Chem. 1 (14) (2003) 2405–2415, https://doi.org/10.1039/b302109b.
[81] M. Paravidino, U. Hanefeld, Enzymatic acylation: assessing the greenness of different acyl donors, Green Chem. 13 (10) (2011) 2651–2657, https://doi.org/10.1039/c1gc15576h.
[82] C.S. Chen, Y. Fujimoto, G. Girdaukas, C.J. Sih, Quantitative analyses of biochemical kinetic resolutions of enantiomers, J. Am. Chem. Soc. 104 (25) (1982) 7294–7299, https://doi.org/10.1021/ja00389a064.
[83] R.J. Kazlauskas, A.N.E. Weissfloch, A.T. Rappaport, L.A. Cuccia, A rule to predict which enantiomer of a secondary alcohol reacts faster in reactions catalyzed by cholesterol esterase, lipase from Pseudomonas cepacia, and lipase from Candida rugosa, J. Org. Chem. 56 (8) (1991) 2656–2665, https://doi.org/10.1021/jo00008a016.
[84] T. Ema, S. Maeno, Y. Takaya, T. Sakai, M. Utaka, Significant effect of acyl groups on enantioselectivity in lipase-catalyzed transesterifications, Tetrahedron: Asymm. 7 (3) (1996) 625–628, https://doi.org/10.1016/0957-4166(96)00049-3.
[85] M.V. Flores, J.J.W. Sewalt, A.E.M. Janssen, A. van der Padt, The nature of fatty acid modifies the equilibrium position in the esterification catalyzed by lipase, Biotechnol. Bioeng. 67 (3) (2000) 364–371, https://doi.org/10.1002/(sici)1097-0290(20000205)67:3<364::aid-bit13>3.0.co;2-r.
[86] N. Melais, L. Aribi-Zouioueche, O. Riant, The effect of the migrating group structure on enantioselectivity in lipase-catalyzed kinetic resolution of 1-phenylethanol, Comptes Rendus Chim. 19 (8) (2016) 971–977, https://doi.org/10.1016/j.crci.2016.05.002.
[87] J. Noro, T.G. Castro, A. Cavaco-Paulo, C. Silva, Substrate hydrophobicity and enzyme modifiers play a major role in the activity of lipase from Thermomyces lanuginosus, Catal. Sci. Technol. 10 (2020) 5913–5924, https://doi.org/10.1039/d0cy00912a.
[88] M. Martinelle, M. Holmquist, K. Hult, On the interfacial activation of Candida antarctica lipase A and B as compared with Humicola lanuginosa lipase, Biochim. Biophys. Acta (BBA) - Lipids Lipid Metabol. 1258 (3) (1995) 272–276, https://doi.org/10.1016/0005-2760(95)00131-u.
[89] J. Ottosson, K. Hult, Influence of acyl chain length on the enantioselectivity of Candida antarctica lipase B and its thermodynamic components in kinetic resolution of sec-alcohols, J. Mol. Catal., B Enzym. 11 (4–6) (2001) 1025–1028, https://doi.org/10.1016/s1381-1177(00)00088-6.
[90] T.M. Donohue, D.J. Tuma, M.F. Sorrell, Acetaldehyde adducts with proteins: binding of [14C]acetaldehyde to serum albumin, Arch. Biochem. Biophys. 220 (1) (1983) 239–246, https://doi.org/10.1016/0003-9861(83)90406-X.
[91] D.J. Tuma, M.R. Newman, T.M. Donohue, M.F. Sorrell, Covalent binding of acetaldehyde to proteins: participation of lysine residues, Alcoholism: Clin. Exp. Res. 11 (6) (1987) 579–584, https://doi.org/10.1111/j.1530-0277.1987.tb00178.x.
[92] A.M. Klibanov, Improving enzymes by using them in organic solvents, Nature 409 (6817) (2001) 241–246, https://doi.org/10.1038/35051719.
[93] Y. Kitamoto, Y. Kuruma, K. Suzuki, T. Hattori, Effect of solvent polarity on enantioselectivity in Candida antarctica lipase B catalyzed kinetic resolution of primary and secondary alcohols, J. Org. Chem. 80 (1) (2015) 521–527, https://doi.org/10.1021/jo502521e.
[94] P.A. Fitzpatrick, A.M. Klibanov, How can the solvent affect enzyme enantioselectivity? J. Am. Chem. Soc. 113 (8) (1991) 3166–3171, https://doi.org/10.1021/ja00008a054.
[95] X. Li, L. Xu, G. Wang, H. Zhang, Y. Yan, Conformation studies on Burkholderia cenocepacia lipase via resolution of racemic 1-phenylethanol in non-aqueous medium and its process optimization, Proc. Biochem. 48 (12) (2013) 1905–1913, https://doi.org/10.1016/j.procbio.2013.09.001.
[96] E. Xun, J. Wang, H. Zhang, G. Chen, H. Yue, J. Zhao, L. Wang, Z. Wang, Resolution of N-hydroxymethyl vince lactam catalyzed by lipase in organic solvent, J. Chem. Technol. Biotechnol. 88 (5) (2013) 904–909, https://doi.org/10.1002/jctb.3919.
[97] L.S. Chua, M.R. Sarmidi, Effect of solvent and initial water content on (R, S)-1-phenylethanol resolution, Enzym. Microb. Technol. 38 (3-4) (2006) 551–556, https://doi.org/10.1016/j.enzmictec.2005.07.027.
[98] Y. Wang, Q. Li, Z. Zhang, J. Ma, Y. Feng, Solvent effects on the enantioselectivity of the thermophilic lipase QLM in the resolution of (R, S)-2-octanol and (R, S)-2-pentanol, J. Mol. Catal., B Enzym. 56 (2–3) (2009) 146–150, https://doi.org/10.1016/j.molcatb.2008.01.010.
[99] T. Ke, C.R. Wescott, A.M. Klibanov, Prediction of the solvent dependence of enzymatic prochiral selectivity by means of structure-based thermodynamic calculations, J. Am. Chem. Soc. 118 (14) (1996) 3366–3374, https://doi.org/10.1021/ja952674t.
[100] C.R. Wescott, H. Noritomi, A.M. Klibanov, Rational control of enzymatic enantioselectivity through solvation thermodynamics, J. Am. Chem. Soc. 118 (43) (1996) 10365–10370, https://doi.org/10.1021/ja961394q.
[101] C.K. Savile, R.J. Kazlauskas, How substrate solvation contributes to the enantioselectivity of subtilisin toward secondary alcohols, J. Am. Chem. Soc. 127 (35) (2005) 12228–12229, https://doi.org/10.1021/ja0528937.
[102] P.L.A. Overbeeke, J.A. Jongejan, J.J. Heijnen, Solvent effect on lipase enantioselectivity. Evidence for the presence of two thermodynamic states, Biotechnol. Bioeng. 70 (3) (2000) 278–290, https://doi.org/10.1002/1097-0290(20001105)70:3<278::aid-bit5>3.0.co;2-i.

[103] G. Carrea, S. Riva, Properties and synthetic applications of enzymes in organic solvents, Angew. Chem. Int. Ed. 39 (13) (2000) 2226–2254, https://doi.org/10.1002/1521-3773(20000703)39:13<2226::aid-anie2226>3.0.co;2-l.
[104] C. Capello, U. Fischer, K. Hungerbühler, What is a green solvent? A comprehensive framework for the environmental assessment of solvents, Green Chem. 9 (9) (2007) 927–934, https://doi.org/10.1039/b617536h.
[105] K. Alfonsi, J. Colberg, P.J. Dunn, T. Fevig, S. Jennings, T.A. Johnson, H.P. Kleine, C. Knight, M.A. Nagy, D.A. Perry, M. Stefaniak, Green chemistry tools to influence a medicinal chemistry and research chemistry based organisation, Green Chem. 10 (1) (2008) 31–36, https://doi.org/10.1039/b711717e.
[106] P.G. Jessop, Searching for green solvents, Green Chem. 13 (6) (2011) 1391–1398, https://doi.org/10.1039/c0gc00797h.
[107] D. Prat, O. Pardigon, H.-W. Flemming, S. Letestu, V. Ducandas, P. Isnard, E. Guntrum, T. Senac, S. Ruisseau, P. Cruciani, P. Hosek, Sanofi's solvent selection guide: a step toward more sustainable processes, Org. Proc. Res. Dev. 17 (12) (2013) 1517–1525, https://doi.org/10.1021/op4002565.
[108] C.M. Alder, J.D. Hayler, R.K. Henderson, A.M. Redman, L. Shukla, L.E. Shuster, H. F. Sneddon, Updating and further expanding GSK's solvent sustainability guide, Green Chem. 18 (13) (2016) 3879–3890, https://doi.org/10.1039/c6gc00611f.
[109] F.P. Byrne, S. Jin, G. Paggiola, T.H.M. Petchey, J.H. Clark, T.J. Farmer, A.J. Hunt, C. Robert McElroy, J. Sherwood, Tools and techniques for solvent selection: green solvent selection guides, Sus. Chem. Proc. 4 (1) (2016), https://doi.org/10.1186/s40508-016-0051-z.
[110] D. Prat, A. Wells, J. Hayler, H. Sneddon, C.R. McElroy, S. Abou-Shehada, P. J. Dunn, CHEM21 selection guide of classical- and less classical-solvents, Green Chem. 18 (1) (2016) 288–296, https://doi.org/10.1039/c5gc01008j.
[111] M. Tobiszewski, J. Namieśnik, F. Pena-Pereira, Environmental risk-based ranking of solvents using the combination of a multimedia model and multi-criteria decision analysis, Green Chem. 19 (4) (2017) 1034–1042, https://doi.org/10.1039/c6gc03424a.
[112] A.O. Magnusson, M. Takwa, A. Hamberg, K. Hult, An S-selective lipase was created by rational redesign and the enantioselectivity increased with temperature, Angew. Chem. 44 (29) (2005) 4582–4585, https://doi.org/10.1002/anie.200500971.
[113] L. Brady, A.M. Brzozowski, Z.S. Derewenda, E. Dodson, G. Dodson, S. Tolley, J. P. Turkenburg, L. Christiansen, B. Huge-Jensen, L. Norskov, et al., A serine protease triad forms the catalytic centre of a triacylglycerol lipase, Nature 343 (6260) (1990) 767–770, https://doi.org/10.1038/343767a0.
[114] T.C. Bruice, F.C. Lightstone, Ground state and transition state contributions to the rates of intramolecular and enzymatic reactions, Acc. Chem. Res. 32 (2) (1999) 127–136, https://doi.org/10.1021/ar960131y.
[115] M. Cammenberg, K. Hult, S. Park, Molecular basis for the enhanced lipase-catalyzed N-acylation of 1-phenylethanamine with methoxyacetate, ChemBioChem: Eur. J. Chem. Biol. 7 (11) (2006) 1745–1749, https://doi.org/10.1002/cbic.200600245.
[116] E.B. De Oliveira, C. Humeau, L. Chebil, E.R. Maia, F. Dehez, B. Maigret, M. Ghoul, J.-M. Engasser, A molecular modelling study to rationalize the regioselectivity in acylation of flavonoid glycosides catalyzed by Candida antarctica lipase B, J. Mol. Catal., B Enzym. 59 (1–3) (2009) 96–105, https://doi.org/10.1016/j.molcatb.2009.01.011.
[117] F. Ferrari, C. Paris, B. Maigret, C. Bidouil, S. Delaunay, C. Humeau, I. Chevalot, Molecular rules for chemo- and regio-selectivity of Candida antarctica lipase B in peptide acylation reactions, J. Mol. Catal., B Enzym. 101 (2014) 122–132, https://doi.org/10.1016/j.molcatb.2013.12.007.
[118] L.J. Farrugia, WinGXandORTEP for Windows: an update, J. App. Cryst. 45 (4) (2012) 849–854, https://doi.org/10.1107/s0021889812029111.